

## **Distribution Agreement**

In presenting this thesis as a partial fulfillment of the requirements for a degree from Emory University, I hereby grant to Emory University and its agents the non-exclusive license to archive, make accessible, and display my thesis in whole or in part in all forms of media, now or hereafter now, including display on the World Wide Web. I understand that I may select some access restrictions as part of the online submission of this thesis. I retain all ownership rights to the copyright of the thesis. I also retain the right to use in future works (such as articles or books) all or part of this thesis.

Jillian Rankin

December 4, 2020

Investigating Gentamicin Mechanism of Action with Fluorescence Microscopy: Relationships  
between Colony Growth, Antibiotic Accumulation, and Membrane Permeability

by

Jillian Rankin

Dr. Minsu Kim  
Adviser

Department of Physics

Dr. Minsu Kim  
Adviser

Dr. Kathleen Campbell  
Committee Member

Dr. Connie Roth  
Committee Member

Dr. Daniel Weissman  
Committee Member

2020

Investigating Gentamicin Mechanism of Action with Fluorescence Microscopy: Relationships  
between Colony Growth, Antibiotic Accumulation, and Membrane Permeability

by

Jillian Rankin

Dr. Minsu Kim

Adviser

An abstract of  
a thesis submitted to the Faculty of Emory College of Arts and Sciences  
of Emory University in partial fulfillment  
of the requirements of the degree of  
Bachelor of Arts with Honors

Department of Physics

2020

## Abstract

### Investigating Gentamicin Mechanism of Action with Fluorescence Microscopy: Relationships between Colony Growth, Antibiotic Accumulation, and Membrane Permeability

By Jillian Rankin

Aminoglycosides constitute a powerful, broad-spectrum class of antibiotics. While aminoglycosides are known to exert their antimicrobial activity through ribosome targeting, the precise mechanism of action through which they produce cell death remains undefined. In particular, there is no clear scientific consensus regarding the role of membrane damage in initiating growth arrest. In this study, we probed aminoglycoside mechanism of action by using fluorescence microscopy to evaluate the interrelationships between membrane damage, growth arrest, and antibiotic accumulation in *Escherichia coli* microcolonies. A fluorophore-conjugated aminoglycoside, gentamicin-Texas Red (GTTR), was used to assess antibiotic accumulation, while SYTOX Green, a nucleic acid stain impermeant to living cells, was used to assess membrane permeability. To further clarify the role of membrane integrity in influencing growth inhibition, treatment groups with variable degrees of induced membrane permeability were compared. Specifically, given that magnesium availability is known to influence outer membrane stability for Gram-negative organisms, colonies cultured in magnesium-supplemented conditions were compared against those cultured in relatively low magnesium conditions. Furthermore, outcomes for colonies treated with colistin, an antibiotic known to induce membrane damage, were compared against those of magnesium-supplemented colonies. We found that, in the context of gentamicin treatment, both low magnesium growth conditions and treatment with colistin induced greater degrees of membrane permeability throughout the experimental timeline, as well as increased rates and extents of gentamicin accumulation, relative to the magnesium-supplemented group. However, we found that these outcomes were not reliable predictors of growth rate or the onset of growth inhibition. Furthermore, our analysis of the temporal relationships between changes in membrane permeability, accumulation, and growth inhibition suggests that the onset of significant losses in membrane integrity are not required to initiate growth arrest. Additional study is required to further clarify the role of membrane damage in gentamicin-induced growth arrest and to ultimately delineate the precise mechanism of action of aminoglycoside antibiotics.

Investigating Gentamicin Mechanism of Action with Fluorescence Microscopy: Relationships  
between Colony Growth, Antibiotic Accumulation, and Membrane Permeability

by

Jillian Rankin

Dr. Minsu Kim

Adviser

A thesis submitted to the Faculty of Emory College of Arts and Sciences  
of Emory University in partial fulfillment  
of the requirements of the degree of  
Bachelor of Arts with Honors

Department of Physics

2020

## Acknowledgements

I would like to first thank Dr. Minsu Kim for allowing me the opportunity to complete this thesis under his supervision and, in doing so, participate in undergraduate research at Emory. This experience has been integral to my growth as a scholar and has provided me with invaluable exposure to the larger scientific community and research process. In addition to the time, resources, insight, and guidance which Dr. Kim has shared with me, I am immensely grateful for his faith in my ability to successfully complete this thesis despite the semester's limitations. This work would not have been possible without his support.

I would also like to acknowledge the significant role of Dr. Tatsuya Akiyama in making possible the realization of this endeavor. The foundation of this thesis is the analysis of microscope images generated by Dr. Akiyama through his work in the laboratory. In the context of the onset of COVID-19 this year, I would not have been able to author this thesis without access to Dr. Akiyama's images or an understanding of his recent work. Beyond his technical contributions, Dr. Akiyama has generously shared his time, expertise, and insight, assisting me in considering the context and greater implications of my findings through shared discussion and reflection. During our many meetings, I always felt encouraged to ask questions, delve deeper into my analysis, and continue to grasp at the truths underlying this research. In this sense, Dr. Akiyama has inspired me by displaying what I believe to be the qualities of a true scientist. Finally, Dr. Akiyama's invariable encouragement and kindness has made the production of this work manageable in difficult times, and engaging, exciting, and rewarding throughout the rest.

I would like to thank Dr. Campbell, Dr. Roth, and Dr. Weissman for supporting my growth and progress as a student of the sciences by serving as committee members for the evaluation of this thesis. Beyond this, Dr. Roth and Dr. Weissman have provided me with excellent academic instruction that has strengthened my ability to understand, analyze, and critically evaluate scientific data and theory. Dr. Campbell has served as an influential mentor and advisor, offering guidance and insight that has positively shaped the trajectory of my academic development.

I would like to thank the staff at Emory University's Woodruff Library and Woodruff Health Sciences Library. These individuals were amongst the few with whom I interacted on campus during the semester over which this thesis was written. Their routine kindness provided me with a sense of warmth and normality that helped me to maintain steady progress towards the completion of this work.

Finally, I would like to thank Dr. Frankie White and Dr. Thomas Albrecht-Schmitt, my research mentors at Florida State University. Their support and mentorship during a highly influential period of my undergraduate education has proved to be integral in shaping the ultimate trajectory of my academic career. By instilling within me an intellectual curiosity, enthusiasm for research, and confidence in my ability to make positive contributions to science, their lasting influence has remained a powerful source of inspiration.

## Table of Contents

CHAPTER I. BACKGROUND .....	1
Introduction to Aminoglycosides .....	1
Ribosome-Targeting by Aminoglycosides.....	1
Proposed Mechanisms of Aminoglycoside Bactericidal Activity .....	2
Implications .....	3
CHAPTER II. EXPERIMENTAL APPROACH .....	5
Motivation .....	5
Use of Gentamicin .....	5
Use of Fluorescence Microscopy .....	7
Membrane Permeability Treatments .....	8
CHAPTER III. METHODS .....	11
Experimental Procedure .....	11
Image Analysis .....	16
Statistical Analysis .....	27
Accounting for Colony Heterogeneity .....	28
CHAPTER IV. RESULTS .....	30
General Findings .....	30
Measures of Membrane Permeability .....	31
Measures of Gentamicin Accumulation .....	36

Measures of Growth and Growth Inhibition .....	42
Relationships between Permeability, Accumulation, and Early Growth.....	45
Relationships between Permeability, Accumulation, and Growth Inhibition .....	49
CHAPTER V. DISCUSSION .....	57
Summary and Implications .....	57
Future Directions .....	60
APPENDIX A. COLONY DATA IN THE CONTEXT OF CELL HETEROGENEITY .....	63
APPENDIX B. TABLES .....	66
REFERENCES .....	71

## CHAPTER I

### BACKGROUND

#### Introduction to Aminoglycosides

Aminoglycosides are a powerful, broad spectrum class of antibiotics. The first aminoglycoside to be used in clinical practice, streptomycin, was discovered in 1944 after isolation from *Streptomyces griseus* (Schatz et. al., 1944; Serio et. al., 2018). A number of additional aminoglycosides were subsequently isolated or synthesized, including neomycin, kanamycin, gentamicin, netilmicin, tobramycin, and amikacin (Krause et. al., 2016). Amongst those commonly employed in clinical practice, members of the aminoglycoside class have been critically important to the treatment of serious infections in neonatal and pediatric settings, as well as for tuberculosis, respiratory infections associated with cystic fibrosis, and in various surgical settings (Germovsek, 2017). Furthermore, there is evidence that they may serve as useful alternatives in certain cases of multi-drug resistant urinary tract infection (Bader et. al., 2017).

#### Ribosome-Targeting by Aminoglycosides

The primary mechanism of action associated with aminoglycoside antibiotic activity is the disruption of protein synthesis through ribosome-targeting (Krause et. al., 2016). A critical

functional unit of both prokaryotic and eukaryotic life, the ribosome is responsible for the translation of mRNA into proteins, which then go on to influence nearly every aspect of cellular structure and function. Given the global influence of protein synthesis on cellular processes, the ability of aminoglycosides to target ribosomal activity makes their mechanism of action and associated disruption to cellular function an ongoing focus of scientific inquiry.

Structural commonalities of members of the aminoglycoside class include multi-ring carbon backbones with amino and hydroxyl group moieties. The fact that both amino and hydroxyl groups are protonated at biological pH is important to aminoglycoside antibiotic activity (Kotra et. al., 2000). This is especially true for the process of ribosome-targeting, as aminoglycoside affinity for rRNA can be primarily attributed to electrostatic attraction between the polycationic antibiotic and negatively charged phosphate backbone of nucleic acid (Fourmy et. al., 1996). It is now widely accepted that the specific site of aminoglycoside binding is at the A site on 16S rRNA of the 30S ribosomal subunit (Krause et. al., 2016). This is considered to be the source of the disruption of protein synthesis and production of mistranslated proteins observed in susceptible bacteria under treatment with aminoglycosides.

### Proposed Mechanisms of Aminoglycoside Bactericidal Activity

Surprisingly, despite the extensive research conducted on aminoglycoside mechanism of action, there is still a conspicuous lack of scientific consensus regarding the precise processes through which aminoglycosides exert their antimicrobial activity. While membrane damage is a well-documented occurrence in the course of treatment with aminoglycosides (Anand et. al., 1960), there is controversy regarding the source of membrane damage and the existence of a causal relationship between membrane damage and cell death. Early explanations implicating the role of

aminoglycoside-induced membrane damage included the proposition that incorporation of mistranslated proteins in the cell membrane was the causal agent of cell death (Davis et. al., 1986). This could be explained as a positive feedback loop: mistranslated proteins produce channels in the membrane, antibiotic uptake and subsequent production of mistranslated proteins is accelerated, and an eventual irreversible loss of membrane integrity triggers cell death (Davis, 1987). Similar observations related to the relationship between phases of antibiotic uptake and changes in membrane permeability have been used as evidence to suggest that the ultimate cause of cell death is the irreversible saturation of ribosomes (Vakulenko and Mobashery, 2003). An additional explanation is that antibiotic accumulation leads to a gradual loss of membrane potential ( $\Delta\Psi$ ), which ultimately causes cell death as the cell can no longer maintain homeostatic equilibrium with its environment (Bryan and Kwan, 1983). More recent studies have suggested that protein mistranslation and trafficking across the cell membrane results in activation of a stress response system that kills the cell through the production of hydroxyl radicals (Kohanski et. al., 2008). At present, a complete explanation of aminoglycoside mechanism of action is still lacking in the literature. It is clear that further study on this topic is warranted.

### Implications

Investigation into these matters is not trivial. Despite the broad range of potential therapeutic applications of aminoglycoside antibiotics, the extent of their current clinical use is limited. While the killing efficacy of certain classes of antibiotics, such as beta-lactams and macrolides, is based on the amount of time that the bacterial target is exposed to the antibiotic, that of aminoglycosides is said to be concentration-dependent (Quintiliani, 2001). By definition, a consequence of this is that optimal antibacterial activity is seen at relatively high antibiotic

concentrations, requiring doses large enough to clinically produce these concentrations in the serum. However, this becomes problematic when considering the observed nephro- and ototoxicity of aminoglycoside antibiotics. In the context of gentamicin specifically, even early studies on clinical efficacy and safety indicated risk for dose-dependent ototoxicity (Wersäll et. al., 1969), as well as for the exacerbation of existing impairments in renal function (Gary et. al., 1976), now also known to be influenced by dose (Awodele et. al., 2015). Despite recent improvements to dosing regimens (Freeman et. al., 1997; Turnidge, 2003; Mui, 2012), these potentially severe outcomes have resulted in decreased utilization of aminoglycoside antibiotics in favor of those that are better-tolerated or with reduced potential for injurious side effects (Blam and Hammer, 1997). It is certainly possible that the toxicities associated with treatment could be mitigated by alterations to drug dosing, prescription of aminoglycosides in conjunction with synergistic antimicrobial agents, or other improvements in clinical application. The development of such advances would almost undoubtedly be hastened by an improved understanding of mechanism of action.

## CHAPTER II

### EXPERIMENTAL APPROACH

#### Motivation

Given the lack of clear understanding of aminoglycoside mechanism of action, further investigation into the sequence of relevant biological events surrounding growth inhibition is warranted. In this study, we examine the relationship between cell growth and growth inhibition, antibiotic accumulation, and membrane permeability changes in *Escherichia coli* microcolonies during treatment with an aminoglycoside antibiotic, gentamicin, to assess whether a causal link between membrane damage and subsequent growth arrest can be supported. We further perturb and probe this system by inducing changes to membrane permeability in order to provide additional insight into the relationship between these events.

#### Use of Gentamicin

Gentamicin is a particularly important aminoglycoside that has been the focus of extensive scholarly inquiry. Chemically, what is known as gentamicin is actually a mixture of five structurally similar (but distinct) isomers derived from *Micromonospora* species (Weinstein et. al., 1963). The extent to which these isomers are distinct is limited only to those differences between

three R-group constituents located at a single side chain, which extends from one of gentamicin's three central ring structures (Seidl and Nerad, 1988). The R-group constituents of different gentamicin isomers are summarized below (Figure 1).

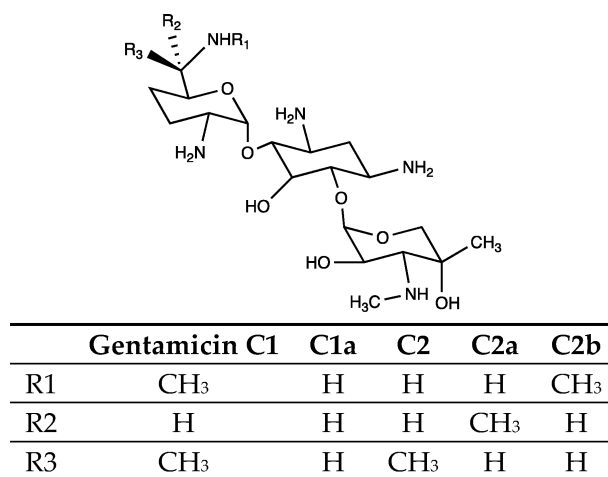


**Figure 1. General structure of gentamicin C components.**<sup>1</sup> Gentamicin is a mixture of five similar, but chemically distinct, isomers.

Given that the variable R-group constituents are either hydrogen or methyl groups, gentamicin isomers have shown predictably minimal differences in chemical or biological behavior when studied individually (Weinstein et. al., 1967).

Amongst aminoglycosides, gentamicin is fascinating in terms of its broad activity against both Gram-negative and Gram-positive organisms (Weinstein et. al., 1963). Since its discovery, gentamicin has been approved by the FDA for use in treating infections by *Klebsiella pneumoniae*,

<sup>1</sup>From “Exclusive Production of Gentamicin C1a from *Micromonospora purpurea* by Metabolic Engineering,” by Wei et. al., 2019, *Antibiotics*, 8(4), 267. <https://www.mdpi.com/2079-6382/8/4/267/htm>. © 2019 by the authors (Wei et. al.). Licensee MDPI, Basel, Switzerland. This article is an open access article distributed under the terms and conditions of the Creative Commons Attribution (CC BY) license (<http://creativecommons.org/licenses/by/4.0/>). The image displayed above was resized but not modified further.

*Escherichia coli*, *Citrobacter spp.*, *Enterobacteriaceae spp.*, *Pseudomonas spp.*, *Staphylococcus spp.*, and *Serratia marcescens* (Chen et. al., 2014). Given this wide range of applications, it is unsurprising that gentamicin is the most commonly used aminoglycoside antibiotic (Gonzalez and Spencer, 1998). While it is most effective against aerobic Gram-negative bacteria, the activity of gentamicin against certain Gram-positive species has been shown to be enhanced through concomitant use with other antibiotics (Gonzalez and Spencer, 1998). Notably, gentamicin synergy has been observed with clindamycin, vancomycin, and beta-lactams such as penicillin (Watanakunakorn and Bakie, 1973; Soriano and Greenwood, 1979; Brook and Walker, 1985).

Despite extensive study, the problem of elucidating a clear aminoglycoside mechanism of action is certainly reflected in the literature regarding gentamicin activity. Considering the need for these studies in conjunction with gentamicin's wide availability, known synergistic interactions, broad clinical applicability, and extensive prior study and documentation in the literature, gentamicin is a favorable choice of antibiotic for use in this study.

### Use of Fluorescence Microscopy

The use of fluorescence microscopy is an attractive approach for the purposes of this study. While a traditional optical microscope allows visualization of microscopic systems through magnification alone, our use of fluorescence microscopy increases the scope of investigation by taking advantage of biochemical properties of fluorescent dyes. Specific wavelengths of light are used to excite electrons in dye molecules, resulting in subsequent electron relaxation and associated fluorescent emissions. For use as probes in microbiology, these dyes must be designed for specificity to some aspect of biological structure or function. Fortunately, there are many available dyes for use in a wide range of biological applications. Of particular interest to this study

are dyes used to gauge antibiotic accumulation and membrane permeability. The first of these requirements is satisfied with the use of a fluorophore-conjugated gentamicin probe, gentamicin-conjugated Texas Red (GTTR). While the Texas Red component of this probe allows for the visualization of gentamicin uptake and spatial distribution, the antimicrobial effect of gentamicin is not compromised. By observing bacterial colonies over the time course of treatment with gentamicin in the presence of GTTR, we are able to garner useful information regarding the relationship between gentamicin uptake, accumulation, and activity. We are also able to probe the changes in membrane permeability that occur over this timescale by utilizing a second fluorescent dye, SYTOX Green. Impermeable to healthy cells, SYTOX Green will fluoresce upon binding to intracellular nucleic acids after a loss of membrane integrity (Thakur et. al., 2017). By observing SYTOX Green uptake in bacterial colonies over time, it is possible to assess changes in permeabilization that take place during the course of gentamicin treatment. This is particularly important given the aims of this study. By determining the timeline of events related to growth inhibition, gentamicin uptake and accumulation, and changes to membrane integrity, we are able to assess whether a distinct temporal relationship can be found between these events. Furthermore, this would provide evidence for or against the existence of a causal link between the loss of membrane integrity and inhibition of growth.

### Membrane Permeability Treatments

The relationships between growth inhibition, gentamicin accumulation, and membrane permeability can be more clearly elucidated through the use of treatment groups known to influence membrane permeability.

While the cell envelope of Gram-negative bacterial cells consists of an outer membrane, peptidoglycan cell wall, and inner membrane, the outer membrane is the primary protective barrier (Hancock, 1984). The presence of lipopolysaccharides is characteristic of the outer membrane and is important in describing membrane structure and integrity (Wilkinson, 1996). In particular, the electrostatic interactions between lipopolysaccharides and divalent cations are a significant source of membrane stability (Nikaido, 2003; Smart et. al., 2017). The finding that reduced magnesium availability is associated with increased outer membrane permeability offers further support for this conclusion (Hancock, 1984).

Another substance with known effects on membrane permeability is colistin, an antibiotic which exerts its bactericidal activity by directly inducing a loss of cell membrane integrity. The polycationic charges associated with colistin's numerous amino groups allow for binding to phosphate groups on Lipid A, a component of outer membrane lipopolysaccharides. The result is a displacement of membrane-associated divalent cations, allowing for interaction between colistin's acyl group and hydrophobic outer membrane lipids. Colistin can then pass through the outer membrane and, through a similar process, the inner membrane of Gram-negative cells. The result is a loss of membrane integrity that induces cell death (Andrade, 2020).

Both magnesium and colistin are expected to influence the behavior and efficacy of aminoglycosides. In the case of magnesium, this effect is related to the early stages of aminoglycoside activity at the outer membrane. The first phase of aminoglycoside uptake is believed to be the adsorption of the antibiotic to membrane lipopolysaccharides and phospholipids through electrostatic interaction, resulting in the displacement of membrane-bound divalent cations (Taber et. al., 1987). Given that this phase is a prerequisite to antibiotic uptake, increased membrane permeability, both in general and to aminoglycosides, could reasonably be expected in

low-magnesium conditions. Similar results could be expected for aminoglycoside-treated cells also under the influence of colistin treatment. Given the reciprocal relationship between cell membrane integrity and aminoglycoside activity and the known induction of membrane damage by colistin, it is unsurprising that colistin displays synergistic bactericidal activity with aminoglycosides, including gentamicin (Bozkurt-Güzel and Gerçeker, 2012; Lenhard et. al., 2016; Zhou et. al., 2017).

For these reasons, this study was carried out using three treatment groups: magnesium-supplemented, low magnesium, and colistin-treated. Further discussion of conditions for each treatment group is provided in the Methods section. The observed between-treatment variability in membrane integrity allowed for improved clarity in our assessment of the relationships between cell growth inhibition, antibiotic accumulation, and membrane integrity.

## CHAPTER III

### METHODS

#### Experimental Procedure

##### *Antibiotic and Dye Stock Solutions*

Sterile water was used to prepare stock solutions of 50 mg/mL gentamicin, 50 mg/mL colistin, and 25 mM Hoechst dye. These solutions were further diluted for use in experiments. A stock solution of 0.5 mM SYTOX Green in DMSO was prepared. Using the procedure described by Sandoval et. al. (1998), a solution of Texas Red-conjugated gentamicin, known as gentamicin-Texas Red (GTTR), was synthesized at a theoretical concentration of 0.25 mg/mL. The ratio of gentamicin:GTTR present in the solution was approximately 33:1. An experiment was performed to compare growth inhibition of NCM3722 by gentamicin against that of GTTR. Luria-Bertani, Miller (LB) broth supplemented with 10 mM glucose and 1 mM MgSO<sub>4</sub> (LB-GlcMg) was used as the culture medium for this experiment. Results indicated that 60 ng/mL of the non-purified gentamicin and GTTR mixture was equivalent in bactericidal activity to approximately 2 to 3 µg/mL of gentamicin alone.

### *Production of Agarose Pads*

Agarose pads were produced for use in microscope experiments. Four microscope slides were used to create a mold, allowing for the production of agarose pads of approximately 1 mm in thickness. A 4 mL sample of LB-GlcMg broth with 1.5% agarose was melted in a 20 mL vial using a microwave. After allowing the mixture to cool, 3 mL of this solution was placed in a pre-warmed 15 mL tube. GTTR solution was added such that a final concentration of 60 ng/mL GTTR was obtained. SYTOX Green fluorescent dye was added to obtain a final concentration of 1  $\mu$ M. Hoechst dye was added to obtain a final concentration of 1  $\mu$ M. For only the agarose pads produced for use with colistin-treated cells, colistin was also added to the medium for a final colistin concentration of 100 ng/mL. After the addition of the antibiotic(s) and dye solutions, the medium mixture was briefly vortexed and then poured into the mold to form an agarose pad. After solidification of the medium, the resultant agarose pad was sliced to produce the appropriate size to fit a glass coverslip for use in microscope experiments.

### *Bacterial Strains and Growth Conditions*

All experiments were performed using *Escherichia coli* NCM3722 strain. A single, isolated bacterial colony cultured on an LB agar plate was used to inoculate 2 mL LB-GlcMg broth in a 16 x 125 mm borosilicate glass culture tube. After inoculation, the tube was placed in a water bath at 37 °C with continuous shaking at 250 rpm. Cells were incubated overnight for 16-20 hours. For the magnesium-supplemented treatment group, cells were subcultured in 5 mL of pre-warmed LB-GlcMg broth in a 20 x 150 mm borosilicate glass culture tube. Media was inoculated at an initial optical density at 600 nm (OD<sub>600</sub>) of approximately 0.001 and subsequently incubated using a water bath at 37 °C with continuous shaking at 250 rpm. For the low magnesium treatment group,

cells were subcultured by obtaining 5 mL of pre-warmed LB broth supplemented with 10 mM glucose (LB-Glc) in a 20 x 150 mm borosilicate glass culture tube. Media was inoculated for an initial OD600 of approximately 0.001 and subsequently incubated using a water bath at 37 °C with continuous shaking at 250 rpm. For the colistin-treated treatment group, cells were subcultured in 5 mL of pre-warmed LB-GlcMg broth in a 20 x 150 mm borosilicate glass culture tube. Media was inoculated for an initial OD600 of approximately 0.001 and subsequently incubated using a water bath at 37 °C with continuous shaking at 250 rpm. For all growth conditions, the optical density of the liquid culture was measured every 20 to 30 minutes using a Genesys 20 spectrophotometer. For the magnesium-supplemented and low magnesium treatment groups, once optical density measurements reached approximately 0.05, 2  $\mu$ L of cell culture was obtained and placed on a glass coverslip. For the colistin treatment group, once the optical density measurement reached approximately 0.05, colistin was added to the culture to a final concentration of 100 ng/mL. The culture was incubated for an additional 30 minutes in a 37 °C water bath with continuous shaking at 250 rpm. After this incubation period, 2  $\mu$ L of cell culture was obtained and placed on a glass coverslip.

### *Imaging Procedure*

The following imaging procedure was performed for all treatment groups. Agarose pads containing GTTR, SYTOX Green, and Hoechst dye (produced according to the methods described above) were placed onto the glass coverslip containing the added cell culture. Pads were gently flattened using a spatula with a bent tip. A second glass coverslip was gently placed atop the agarose pad; this was considered the start time (Time = 0 minutes) for image collection. The coverslip and sample were placed onto the microscope with an automated XY stage, enclosed in a

37°C incubator to ensure constant temperature conditions. An oil-immersion phase-contrast 60x objective lens was used to obtain phase contrast and fluorescence images, which were taken at 5-minute intervals. Microscope settings were for exposure times of 100 ms for phase contrast, 200 ms for Texas Red, 100 ms for GFPi10<sup>2</sup>, and 100 ms for DAPI<sup>3</sup>.

An example of an image obtained using this procedure is given below (Figure 2). Note that this image represents one frame, a single time point in the image series, of the combined output from all channels.

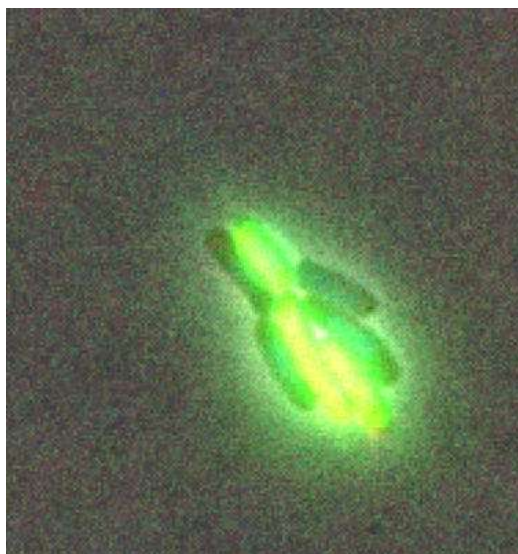


**Figure 2. Example of a composite image produced using fluorescence microscopy.** Composite images combining all channel outputs were the “raw” product produced using the imaging procedure.

---

<sup>2</sup> GFPi10 is a fluorescence microscope setting used for imaging Green Fluorescent Protein (GFP) at 10% laser power. Wild-type GFP has two absorption bands at 395 and 475 nm and one emission peak at 508 nm (Follenius-Wund et. al., 2003). In this experiment, the GFPi10 setting was used to image SYTOX Green, which displays excitation by 450 to 490 nm light and an emission peak at 523 nm (Thermo Fisher Scientific).

<sup>3</sup> DAPI is a fluorescent dye known for its affinity for binding deoxyribonucleic acid (Kapuscinski, 1995). It has an absorption band centered around 360 nm and an emission peak at around 460 nm (Kolozsvari et. al., 2014). Here, the term “DAPI” refers to a microscope set-up using a blue-ultraviolet filter. In this experiment, the DAPI setting was used to image Hoechst dye, which displays excitation by ultraviolet light and emission between 460 to 490 nm (Thermo Fisher Scientific).

The composite image could be separated by channel (Figure 3). The four channels measured phase contrast (Figure 3A), Texas Red fluorescence (Figure 3B), SYTOX Green fluorescence (Figure 3C), and Hoechst dye fluorescence (Figure 3D).

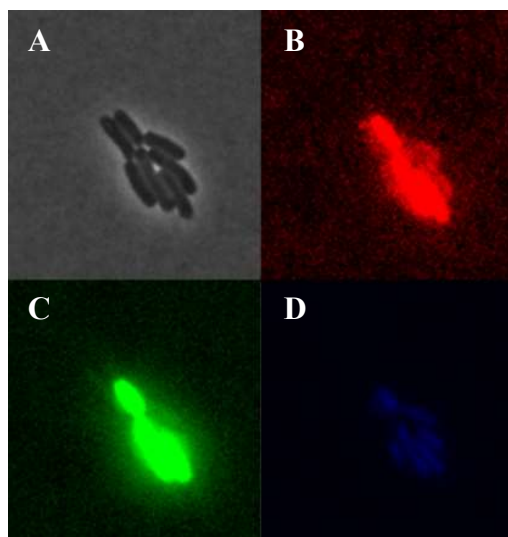


**Figure 3. Example of individual channel images obtained with fluorescence microscopy.** Combined, these channels form the composite image. (A) The phase contrast channel allows for visualization of the bacterial cells. (B) The Texas Red fluorescence channels is used to track gentamicin accumulation. (C) The SYTOX Green fluorescence channel is used to track changes in membrane permeability. (D) The Hoechst dye fluorescence channel is used to show the distribution of nucleic acids but was not used in this analysis.

The phase contrast channel allows the identification of the area occupied by. The area then can be used to track growth over time. The Texas Red channel allows for observation of the spatial and temporal progression of gentamicin accumulation. The SYTOX Green channel allows changes

to membrane permeability to be assessed. The Hoescht dye channel allows for the visualization of the distribution of nucleic acids, but was not used for the purposes of this study.

## Image Analysis

### *Data Collection*

Fiji, an open-source distribution of ImageJ software for scientific image analysis (Schindelin et. al., 2012), was used to collect data from fluorescence microscopy images. Before analysis of each set of images, image properties were set such that pixel size appropriately reflected the true dimensions of the samples, where pixel width and pixel length were equivalent to 0.1083  $\mu\text{m}$ . Image properties were also set such that the time interval between frames was 5 minutes. Channels were split so that colony area selection could be performed using the phase contrast channel; this allowed for selection of colony area in each image frame regardless of any influence of fluorescence. To aid in the selection of colony area, the image threshold was adjusted in image settings. An example of colony area selection using a threshold-adjusted image is depicted below (Figure 4). Images A, B, and C show the area selections at three different time points in the series. Note that later time points were subject to relatively increased proportions of non-cell regions falling within the selected area, seen here as red regions located within the bounds of the selection outlined in yellow. To minimize this influence and ensure the most accurate selection of colony area, threshold adjustments were made throughout this process as needed.

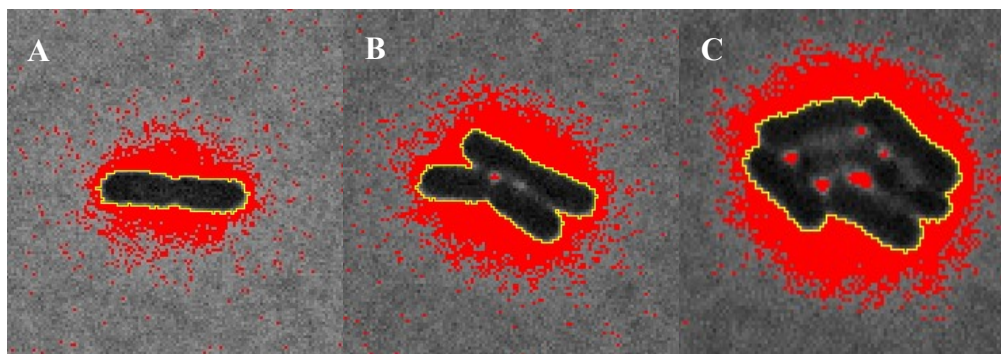


**Figure 4. Colony area selection with threshold-adjusted phase contrast images.** The phase contrast channel was used to collect measurements of colony area. Selected colony area is shown outlined in yellow. For all colonies, this process was performed for each frame in the image series; here, images A, B, and C depict the colony area selection for the same colony at different time points. Threshold was manually adjusted as needed to aid in the process of area selection.

Using this process, the entire colony area was selected and measured for each image frame. These colony area selections were saved as an ROI file, which could then be overlaid on each of the other channels to obtain measurements related to Texas Red, SYTOX Green, and Hoechst dye fluorescence. For each channel, the frame number, colony area, and mean fluorescence intensity values were collected and saved. Given that the colony area followed the same frame-to-frame sequence regardless of channel, the area values were the same for all channel data for a given colony. For each channel, the mean value represented the average fluorescence intensity for all pixels within the selected area. After collection of image data for one colony was complete, the image file, ROI file, and ImageJ software were closed before proceeding with data collection for the next colony. While Hoechst dye fluorescence values were collected, they were not analyzed for this study.

For each colony, the area, Texas Red fluorescence, and SYTOX Green fluorescence values were plotted against time. An example these plotted measurements for a single colony is given below (Figure 5).

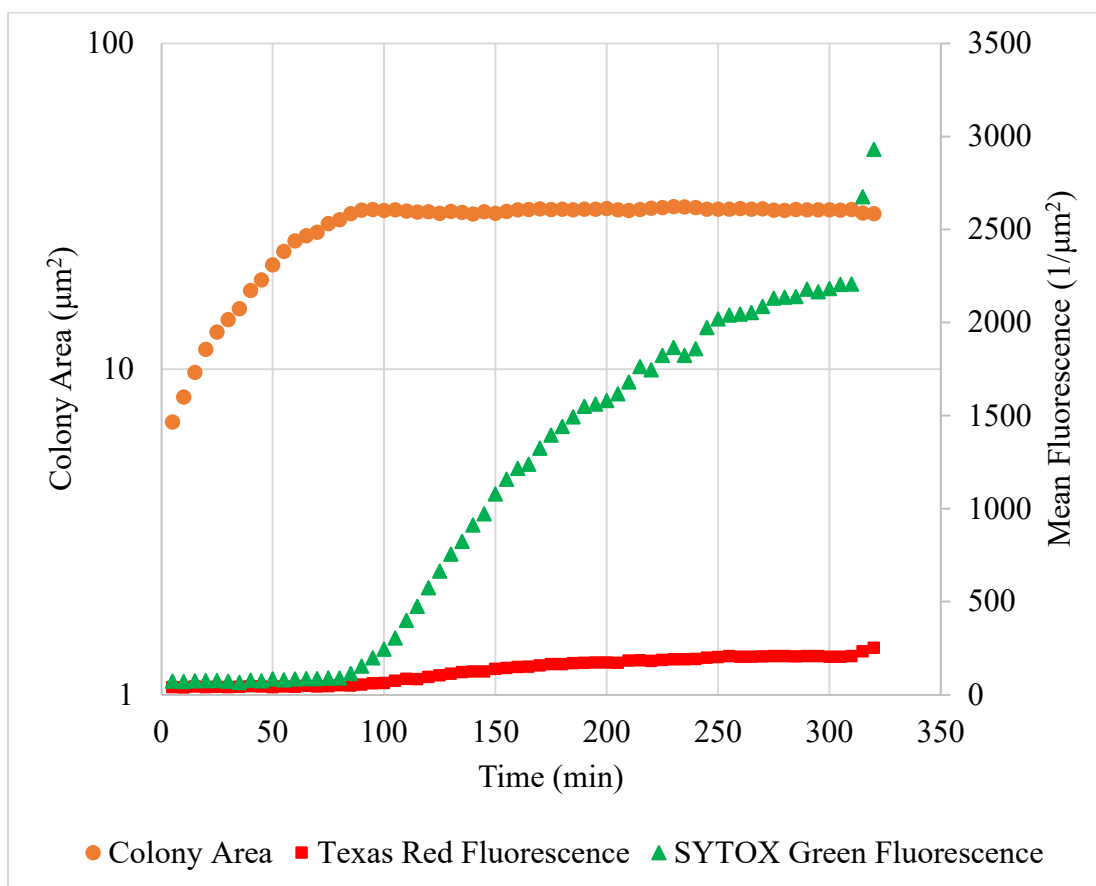


**Figure 5. Example of colony area, Texas Red fluorescence, and SYTOX Green fluorescence trajectories for a single colony.** Colony area is plotted on a logarithmic scale so that the exponential and stationary growth phases can be clearly observed. The SYTOX Green and Texas Red trajectories show how permeability and gentamicin accumulation change over time.

Colony area was plotted on a logarithmic scale so that the exponential and stationary phases were clearly visible. The exponential phase characteristically shows a linear growth trajectory when plotted on a logarithmic scale, as seen in the early time points of colony area data here. The

stationary phase is marked by the cessation of colony growth, as seen in the asymptotic portion of the area curve during the later time points. SYTOX Green and Texas Red fluorescence trajectories show how permeability and gentamicin accumulation change over time.

Between colonies, there was notable heterogeneity between measurement trajectories, particularly in terms of the SYTOX Green and Texas Red fluorescence curves. To quantitatively compare colonies despite these differences, a number of measurements, which could be broadly applied, were devised.

#### *Measurement of Colony Growth Parameters*

The parameters related to colony growth that were collected were time of growth phase transition ( $T_t$ ), time of stationary phase onset ( $T_s$ ), exponential phase growth rate constant, and doubling time.

$T_t$  was determined to be the time point closest to the intersection of the horizontal line tangent to the point at the onset of growth arrest and the linear line through the area points corresponding to the exponential growth phase, linear when viewed on a log scale (Figure 6). As the intersection of these two trajectories (the exponential phase and the stationary phase), this time point represents an approximation for the average onset of growth inhibition across all cells in the colony.

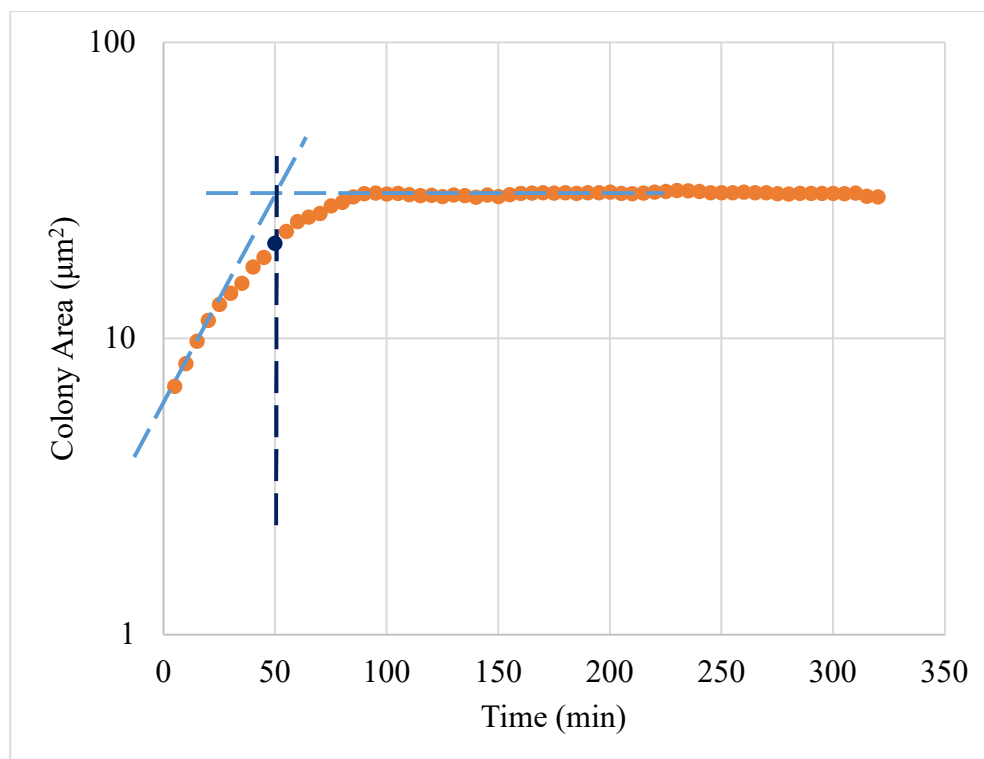


**Figure 6. Time of growth phase transition,  $T_t$ .** The time of growth phase transition was considered to be the time point at which the trajectories for exponential phase growth (diagonal, dashed, light blue line) and stationary phase growth (horizontal, dashed, light blue line) intersect. This time point, displayed here in dark blue, represents an average onset of growth arrest for the single cells in the colony.

$T_s$ , the time of stationary phase onset, was determined to be the first time point at which colony area reached an approximately constant value (Figure 7). This is representative of the time at which all cells in the colony have become growth arrested. Additional information regarding the relationships between  $T_t$ ,  $T_s$  and single-cell growth arrest is presented in Appendix A.

Mean Texas Red fluorescence and mean SYTOX Green fluorescence values at the time  $T_s$  were also collected using the raw data for mean fluorescence.

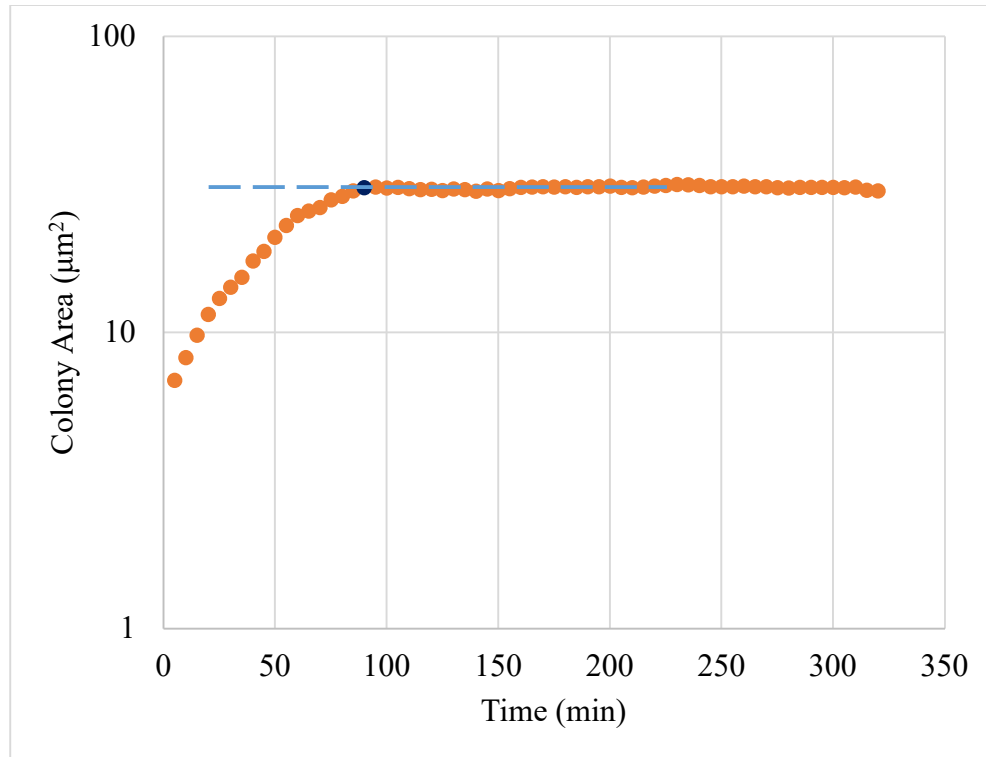


**Figure 7. Time of onset of the stationary phase,  $T_s$ .**  $T_s$  is the first time point at which the colony area reaches an approximately constant value, indicating that all cells in the colony have become growth arrested. Here, the stationary phase trajectory is displayed as a dashed, light blue line. Area at the time  $T_s$  is displayed as a dark blue point.

The exponential phase growth rate constant was found by performing a linear regression over the  $\log_2(\ )$  area and time values during the exponential growth phase (Figure 8). The end point of the exponential growth phase was considered to be the last data point before logarithmic-scale area values diverged from a linear trajectory.

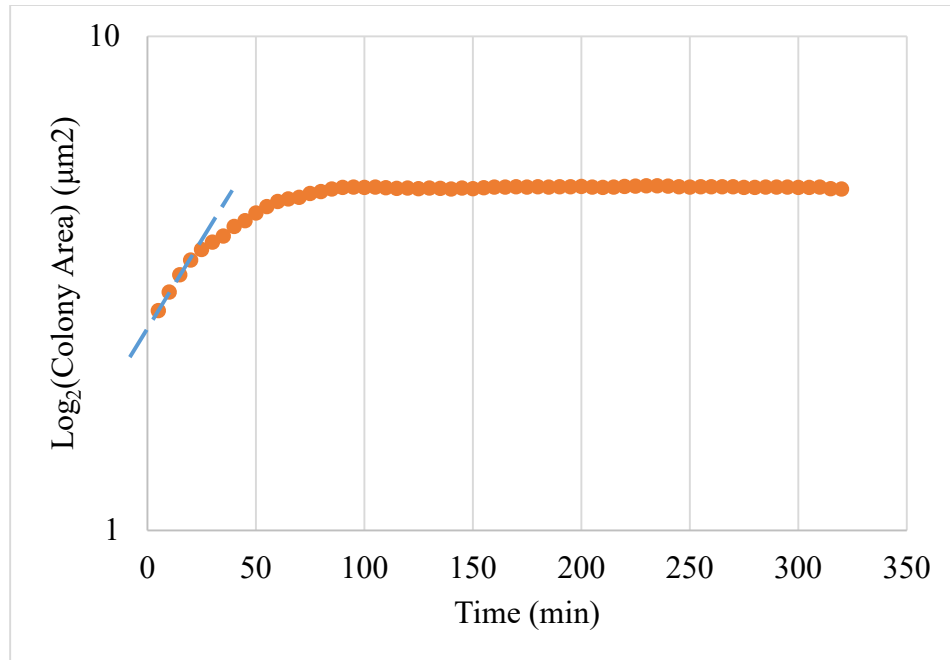


**Figure 8. Determining time points for use in calculation of the growth rate constant.** To find the growth rate constant, a linear regression was performed over the  $\log_2(\ )$  area values corresponding to the exponential growth trajectory, shown here as a dashed, light blue line. For this example, the first four points would be used in the calculation for growth rate constant, as the fifth point significantly diverges from the exponential growth phase trajectory.

The  $\log_2(\ )$  area values were taken for use in calculating the exponential phase rate constant based on the following model for bacterial growth in the exponential phase:

$$N(t) = e^{rt}N(0) = 2^{\frac{t}{T}}N(0)$$

where  $T = \frac{\ln(2)}{r}$  is the doubling time characteristic of the bacterial population and growth conditions (Allen and Waclaw, 2019). This follows from the biological principle that bacteria reproduce through the process of binary fission. Doubling time, or the time between events of

cellular division (time for the bacterial population size to double) was found by taking the inverse of the exponential phase growth rate constant (Todar, 2020).

#### *Measurement of SYTOX Green and Gentamicin-Texas Red Uptake Parameters*

The measured parameters related to SYTOX Green uptake were initial SYTOX Green uptake rate, rapid uptake phase SYTOX uptake rate, time of SYTOX Green rapid uptake phase onset, and maximum SYTOX Green fluorescence. Each of these parameters was measured for each colony in each treatment group.

The maximum SYTOX Green fluorescence was found by selecting the maximum mean SYTOX Green fluorescence value observed during the course of imaging (Figure 9).

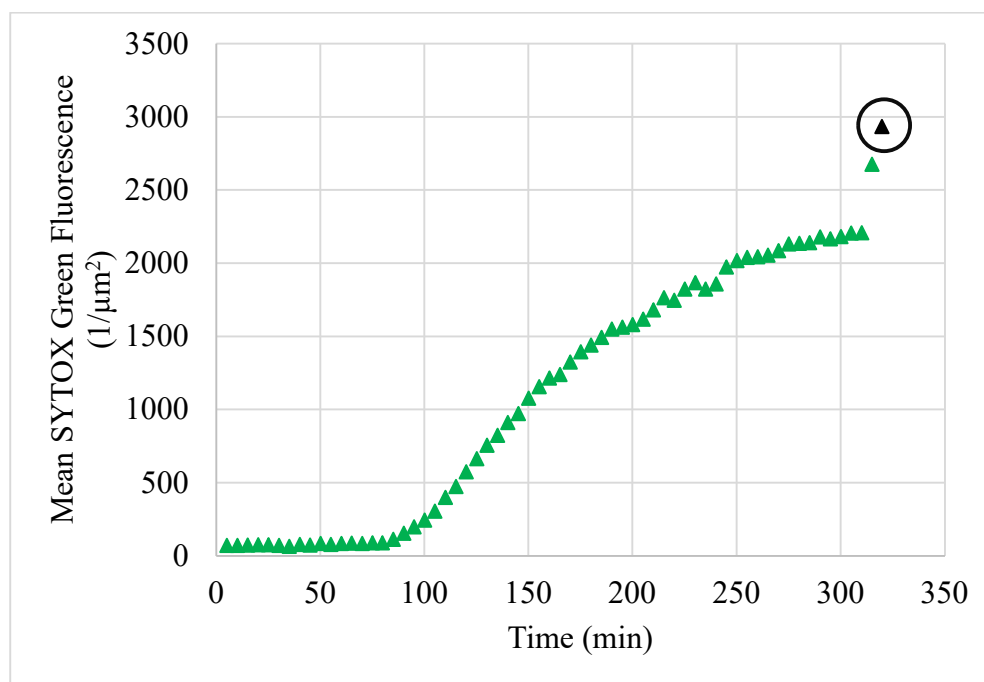


**Figure 9. Maximum SYTOX Green fluorescence.** The maximum SYTOX Green fluorescence (black, circled) is the highest measured value of SYTOX Green fluorescence observed over the course of imaging.

The time of SYTOX Green rapid uptake phase onset was determined to be the last time point before a large spike in SYTOX Green fluorescence occurred (Figure 10).

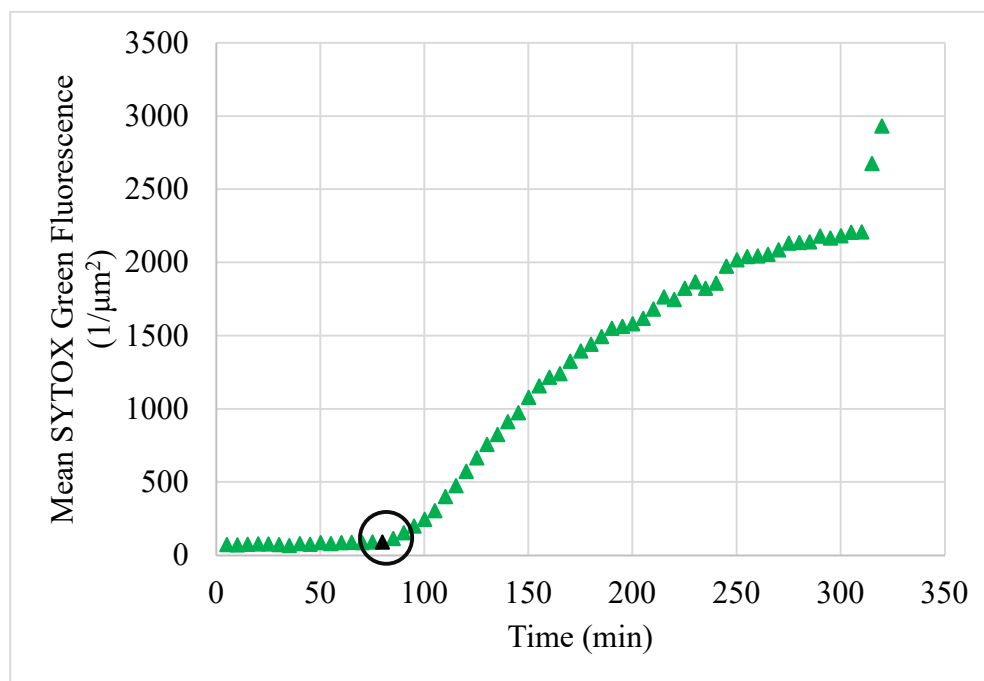


**Figure 10. Time of SYTOX Green rapid uptake phase onset.** The time of SYTOX Green rapid uptake phase onset (black, circled) was determined to be the first time point before the rate of SYTOX Green uptake showed a significant “spike.”

While this point may appear to lie on the initial uptake phase trajectory, it is obvious that the uptake rate change occurred sometime after that time point but before the next. Therefore, given the discrete nature of the data time points, we assume this time point to be a reasonable and consistent approximation of the time of rapid uptake phase onset.

The initial SYTOX Green uptake rate was found by performing a linear regression over mean SYTOX Green fluorescence and time data for time points occurring before the change in

uptake rate. The data points selected for this calculation were found by visually analyzing the SYTOX Green trajectory (Figure 11).

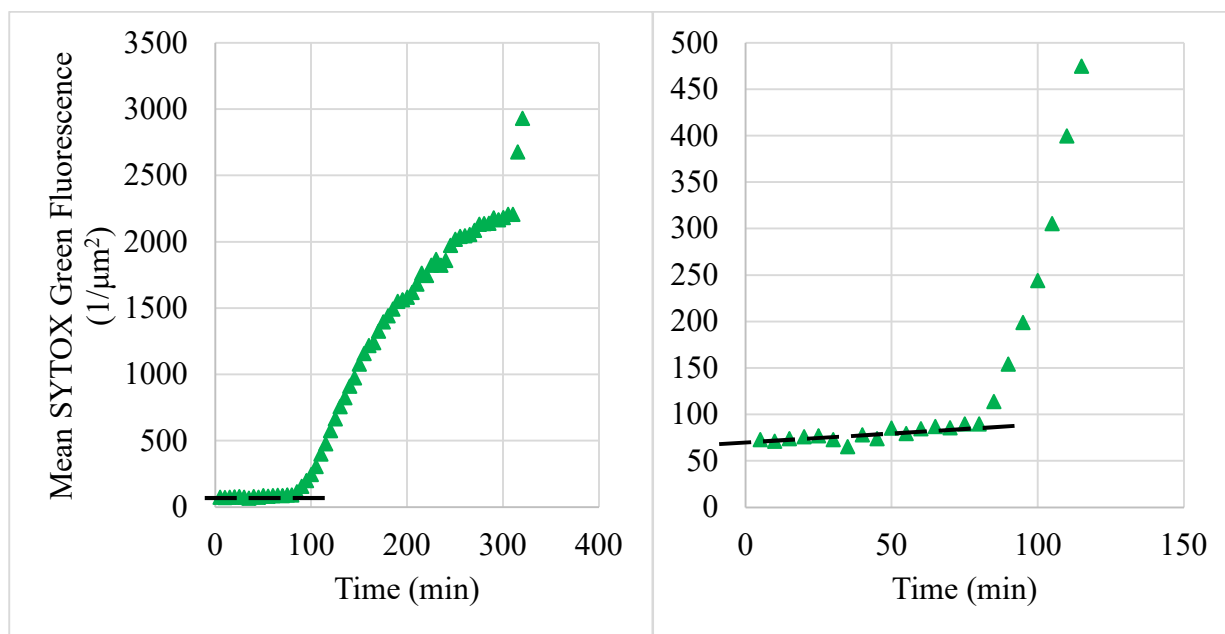


**Figure 11. Selection of points for the calculation of SYTOX Green initial uptake phase.** The time points used for the calculation of SYTOX Green initial uptake rate were those following an approximately linear trajectory during the early stage of SYTOX Green uptake, before a large “spike” in SYTOX Green fluorescence occurred. This trajectory is shown here as a black, dashed line (left). A linear regression was then used to determine the slope of this line, which was the initial uptake rate. To choose the cut-off for inclusion of points in this phase, it was helpful to view early time points on a reduced, or “zoomed-in,” scale (right).

The rapid uptake phase SYTOX Green uptake rate was found by performing a linear regression over mean SYTOX Green fluorescence and time data for time points following an approximately linear trajectory just after the time of rapid uptake phase onset (Figure 12).

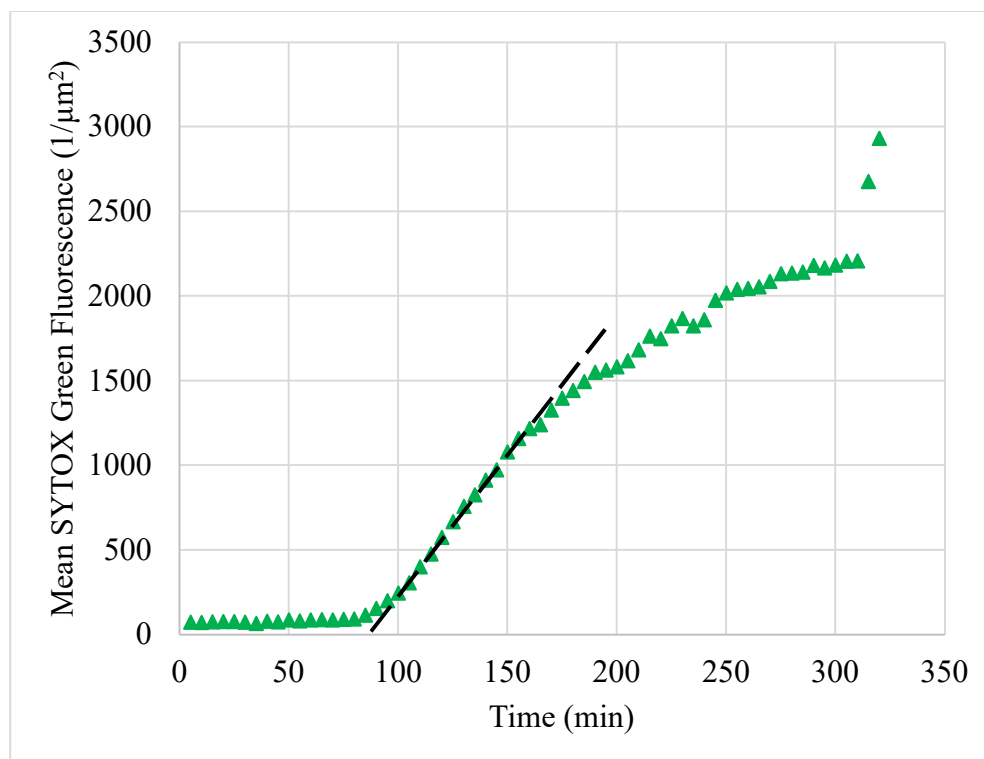


**Figure 12. Selection of points for the calculation of SYTOX Green rapid uptake phase.** The time points used for the calculation of rapid uptake phase SYTOX Green uptake rate were those following an approximately linear trajectory (black, dashed line) just after the onset of the “spike” in SYTOX Green fluorescence values. A linear regression was then used to determine the slope of this line, which was the rapid uptake phase uptake rate.

The measured parameters related to gentamicin accumulation were initial GTTR accumulation rate, rapid uptake phase GTTR accumulation rate, time of GTTR rapid uptake phase onset, and maximum Texas Red fluorescence. Each of these parameters was calculated using the same procedure as was used for the corresponding SYTOX Green parameters.

## Statistical Analysis

After all parameter measurements were collected for each colony in each treatment group, statistical analysis for comparisons between groups was performed using the Mann-Whitney U test. While a T-test is generally used to compare means of two sets of data, it relies on the assumptions that (1) the underlying population data is normally distributed or the sample size is sufficiently large (generally,  $N > 30$ ) and sample data is normally distributed, and (2) the data from the two groups being compared show approximately equivalent variance. In this case, we could not assume that the first condition was met given that the underlying population distributions for the measured parameters were unknown, and sample sizes were too small to determine whether the sample data distributions were normal. We also could not assume that the second condition was met given that the variance of a given measurement was generally not consistent across treatment groups. For these reasons, we employed the Mann-Whitney U test, which is a non-parametric statistical test that does not rely on the above assumptions. It is used to assess whether two sets of data have the same underlying distribution; this is the null hypothesis of the test,  $H_0$ . A statistically significant result indicates that the two sets of data are not likely to have the same underlying distribution; this is the alternative hypothesis of the test,  $H_a$ . This test was used to assess whether there were statistically significant differences between the magnesium-supplemented and other two treatment groups, in terms of each parameter that was measured using the procedure described above.

## Accounting for Colony Heterogeneity

### *Gentamicin-Texas Red and SYTOX Green Uptake Trajectories*

While most of the colonies exhibited uptake trajectories where a linear approximation was the most appropriate choice, there were a small number of cases in which uptake kinetics may have been better modeled by a logarithmic or sigmoidal approximation. In these cases, a linear approximation was performed using the most appropriate data points in order to facilitate the best possible comparison between colonies. For example, in a case where GTTR accumulation during the rapid uptake phase appeared to follow a logarithmic trajectory, a linear regression was performed over the initial, approximately linear portion of this curve. Whenever an appropriate linear approximation could not be made, the colony was excluded from the comparison for that particular measurement.

There were also a small number of colonies for which time of rapid uptake phase onset could not be appropriately assessed. In most cases, this was due to the lack of an observable or otherwise clear rate change for either GTTR accumulation or SYTOX Green uptake. In such cases, these colonies were excluded from comparison for the particular measurement in question.

Scientifically, the exclusion of any data is not ideal as it introduces inherent bias to the results. Unfortunately, given the significant variation between colony trajectories, it was very difficult to construct parameters that could be consistently applied to every colony studied. While the parameters used here were selected and defined so that they could be applied as broadly as possible, future studies should consider whether there are better options that can be used more consistently in order to minimize the exclusion of any individual colony's parameter measurements during data analysis.

### *Fluctuations in Stationary Phase Colony Area*

In some cases, the colony area showed a pattern-less fluctuation in value during the stationary phase. Ideally, we would expect that colony area would be constant or, in some cases, showing a steady decrease during this time. However, some fluctuation was unavoidable due to the discrete nature of pixelated image composition and the propensity of the software to occasionally select a small number of non-colony pixels, or alternatively fail to select the best approximation of true colony area. Adjustments in threshold (which had no bearing on collected data values) were made whenever the accuracy of data selection could benefit from such changes.

### *Cell Heterogeneity*

The process of conducting image analysis made clear the important influence of individual cell growth, uptake, and accumulation trajectories to the heterogeneity observed at the colony level. While analysis of individual cell trajectories was not a focus of this study, one colony of the magnesium-supplemented group was analyzed at the individual cell level to provide insight into interpretation of colony-level data. A discussion of this analysis is presented in Appendix A.

## CHAPTER IV

### RESULTS

#### General Findings

In general, there was notable heterogeneity observed in the measured parameters, both within and between treatment groups. While all colony area trajectories displayed the characteristic exponential and stationary growth phases, the GTTR and SYTOX Green trajectories varied greatly between colonies. In general, these uptake curves could mostly be modeled under an approximation of linear uptake kinetics.

There was no clear timeline of measured events observed consistently between colonies. The times of growth phase transition and onset of stationary phase did not predictably occur either before or after the onset of GTTR rapid uptake phase or SYTOX Green rapid uptake phase. This is discussed in detail later in this chapter.

It is worth noting that, on gross observation, the trajectories of GTTR accumulation and SYTOX Green uptake for colistin-treated colonies appeared to be much more homogenous than were those of the other two treatment groups. The onset of the SYTOX Green rapid uptake phase occurred for all 16 colonies of the colistin-treated group, whereas this was only clearly observed in 11 of the 16 magnesium-supplemented colonies. The trajectory itself appeared to follow the

same shape for all colistin-treated colonies, with a rapid, approximately linear phase of SYTOX Green uptake that peaked and then subsequently decreased later in the timeline. This was not the case for the magnesium-supplemented group, where the rapid uptake phase appeared to vary between being highly linear, approximately exponential, approximately logarithmic, or approximately sigmoidal. While all 10 of the low magnesium colonies showed observable SYTOX Green and GTTR rapid uptake phases, the trajectories varied in appearance in a way similar to those of the magnesium-supplemented group. Colistin-induced homogeneity in these trajectories may be an interesting topic of future study.

### Measures of Membrane Permeability

To determine whether there were differences in membrane permeability by treatment group, initial SYTOX Green uptake rate, SYTOX Green uptake rate during the rapid uptake phase, maximum mean SYTOX Green fluorescence, and time of onset of the rapid uptake phase were assessed for each colony in each treatment group. As expected, there were clear differences in membrane permeability observed between treatment groups throughout the course of gentamicin treatment.

For a given parameter, variation within and between treatment groups is displayed through the use of box and whisker plots. Here, we first display variation observed in SYTOX Green uptake rates. After this rate was measured for all colonies based on their SYTOX Green trajectories, these values were combined by treatment group. The distribution of these values for the magnesium-supplemented group is shown on the left, low-magnesium in the middle, and colistin-treated on the right. The “X” on each box indicates the mean value for that distribution; for example, the “X” on the magnesium-supplemented box shows what the average initial SYTOX Green uptake rate

was for colonies in that group. Similarly, the black horizontal line across the box indicates the median value. The horizontal edges of the box indicate the spread of the middle 50% of the data, where the lower horizontal line represents the data point at the 25<sup>th</sup> percentile and the upper horizontal line represents the data point at the 75<sup>th</sup> percentile. The edges of the “whiskers” represent the minimum and maximum values falling within 1.5 times the interquartile range (IQR) of the median. The IQR is equal to the difference between the 75<sup>th</sup> percentile value and the 25<sup>th</sup> percentile value in the distribution. Outliers, represented here as dots beyond the whisker line, are values that are either less than the median minus 1.5 times the IQR, or greater than the median plus 1.5 times the IQR. Whether there were significant differences between group distributions was assessed using the Mann-Whitney U test. This was performed for a comparison of the magnesium-supplemented and low magnesium treatment groups, as well as for a comparison of the magnesium-supplemented and colistin-treated groups. In the figures below, a “\*” symbol is used to indicate that a significant difference between group distributions was found at the  $\alpha = 0.05$  level. If there was not a significant difference, “n.s.” is used to denote this result.

Given these conventions, we first display the results for the initial and rapid uptake phase SYTOX Green uptake rates (Figure 13 and Figure 14, respectively).

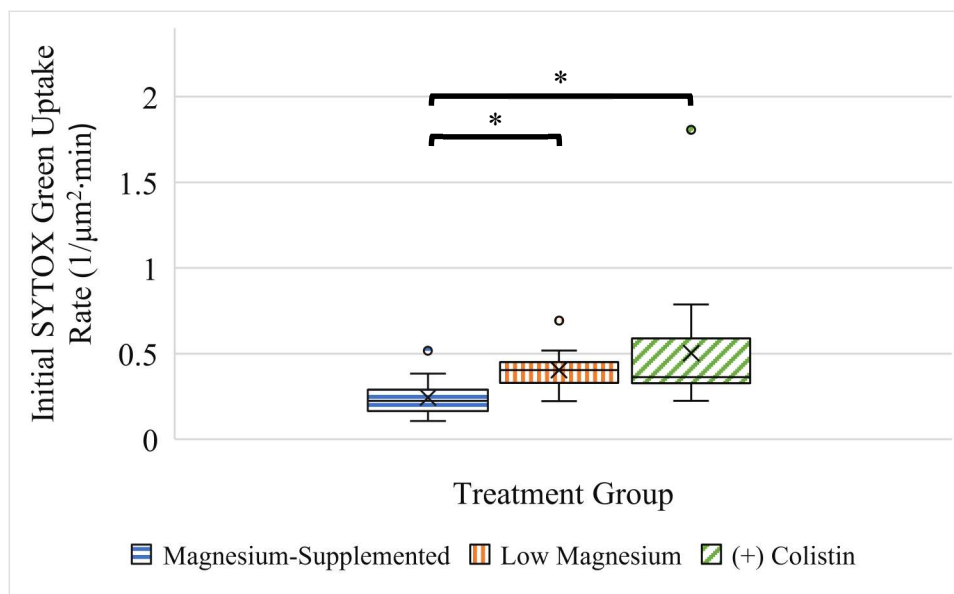


**Figure 13. Initial SYTOX Green uptake rate.** Differences in membrane integrity by group are apparent even in the early stages of gentamicin treatment.

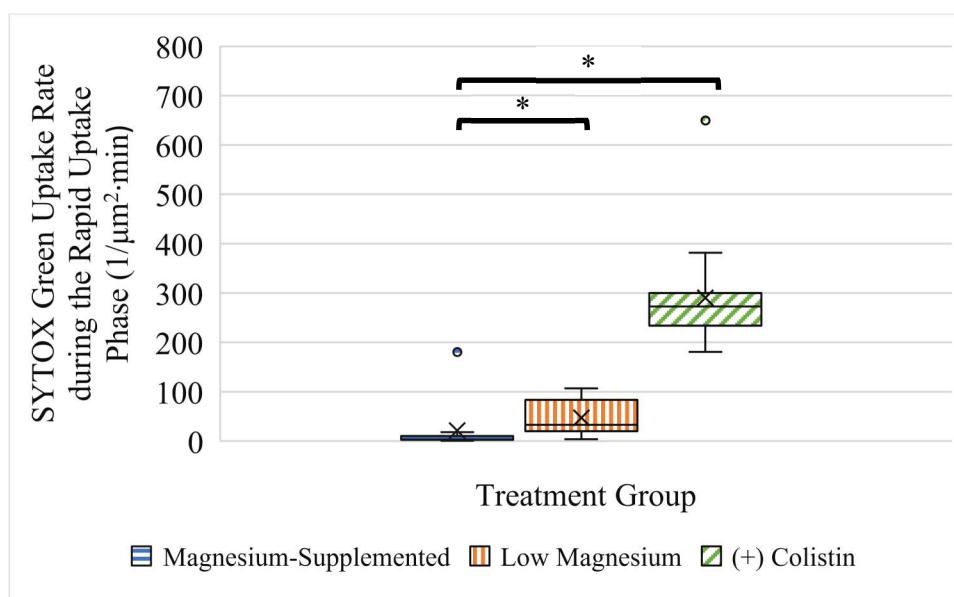


**Figure 14. SYTOX Green uptake rate during the rapid uptake phase.** Changes in membrane permeability are induced by low magnesium conditions or colistin treatment.

As we see, both the low magnesium and colistin-treated groups showed increased SYTOX Green uptake rates during both the initial and rapid uptake phase time periods, relative to those observed for the magnesium-supplemented group. This suggests that membrane permeability is increased for these treatment groups throughout the experimental timeline.

Evidence for differences in membrane permeability between treatment groups was also observed in the results for maximum mean SYTOX Green fluorescence, with the same trend observed as in the two measures of SYTOX Green uptake rate (Figure 15).

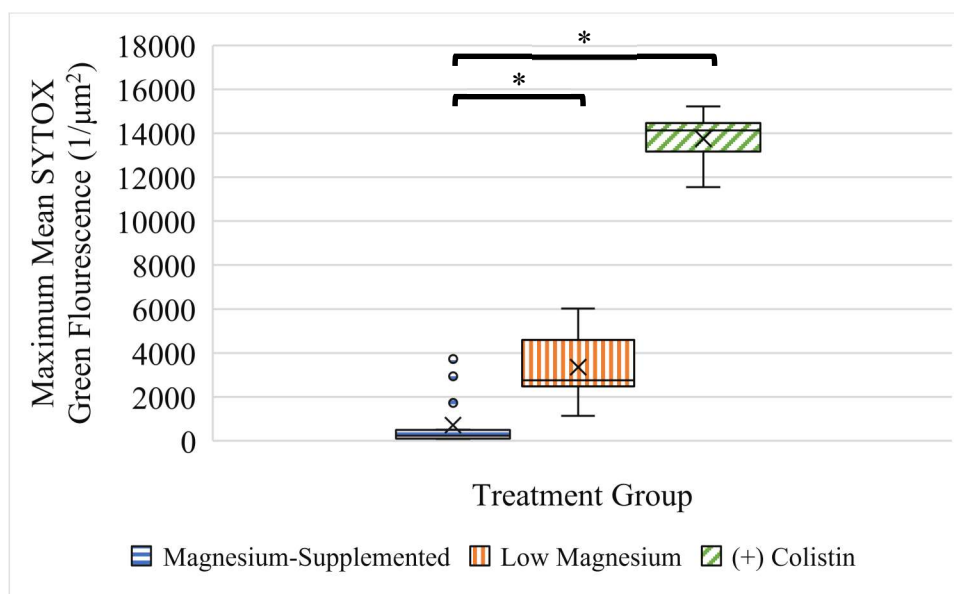


**Figure 15. Maximum mean SYTOX Green fluorescence observed over the course of gentamicin treatment.** The extent of membrane permeability varies by treatment group, greater degrees of membrane permeability noted in both the low magnesium and colistin-treated groups relative to that seen in the magnesium-supplemented group.

Finally, earlier onsets of membrane damage, as indicated by lower values for the time of onset of the SYTOX Green rapid uptake phase, were observed in both the low magnesium and colistin-treated groups relative to the magnesium-supplemented group (Figure 16).

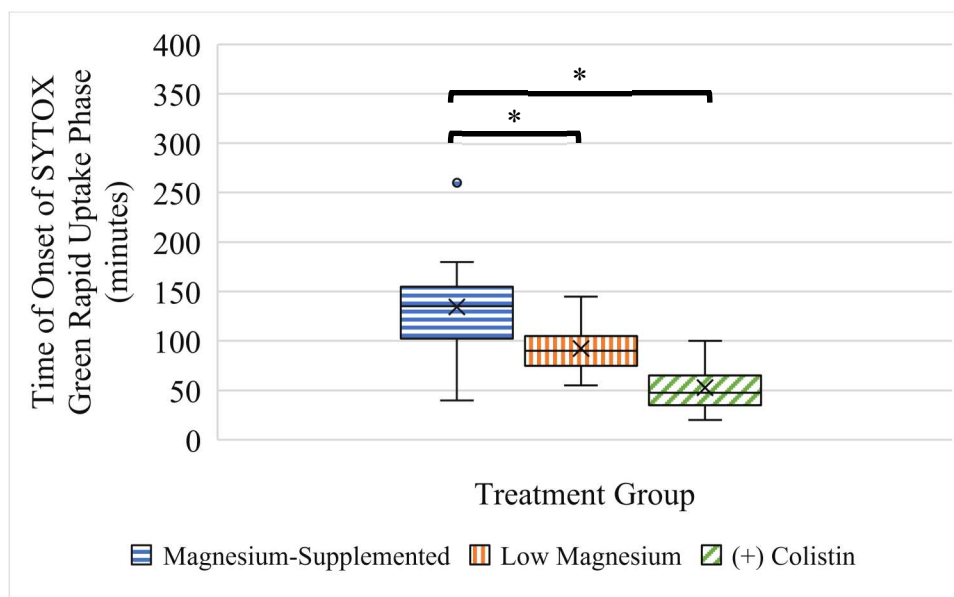


**Figure 16. Time of SYTOX Green rapid uptake phase onset.** The magnesium-supplemented group showed a later loss of membrane integrity relative to that observed in either the low magnesium or colistin-treated groups.

Ultimately, these results were consistent with our expectations that low magnesium conditions, or treatment with colistin, would result in greater extents of membrane destabilization throughout the experimental timeline of gentamicin treatment. To summarize, increased membrane permeability was observed during both the initial stage of SYTOX Green uptake as well as after the onset of the rapid uptake phase. The degree of membrane destabilization was also reflected in the maximum mean SYTOX Green fluorescence values. Finally, membrane permeabilization occurred not only to greater extents, but over an earlier timescale, as evidenced

by earlier onsets of SYTOX Green rapid uptake phase in the low magnesium and colistin-treated groups. These results are summarized quantitatively in Table 1 (Appendix B).

### Measures of Gentamicin Accumulation

To assess how differences in membrane permeability influenced the trajectory and extent of gentamicin uptake and accumulation, the initial GTTR accumulation rate, GTTR accumulation rate during the rapid uptake phase, and maximum mean Texas Red fluorescence were measured for each colony.

The initial GTTR accumulation rate was lower for the magnesium-supplemented treatment group than it was for either the low magnesium or colistin-treated group (Figure 17). A similar result was observed in the GTTR accumulation rate during the rapid uptake phase (Figure 18).

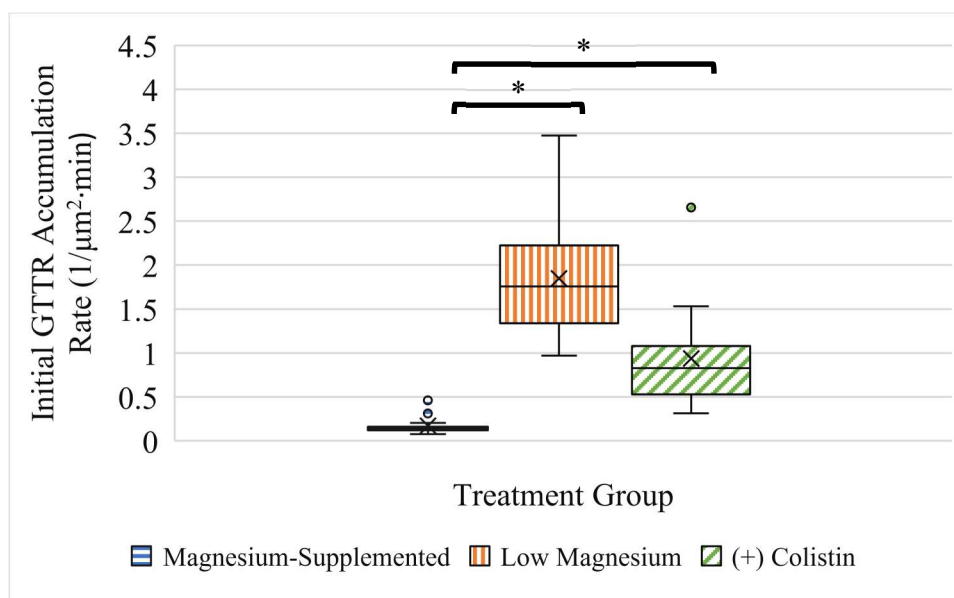


**Figure 17. Initial GTTR accumulation rate.** Initial GTTR accumulation rate varies with induction of changes to membrane permeability, including decreased magnesium availability and treatment with colistin.

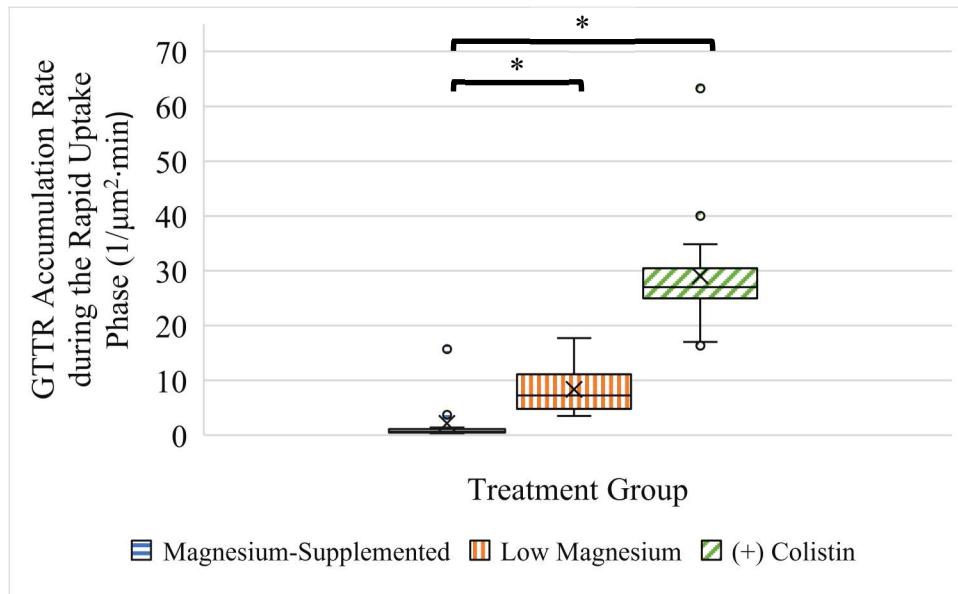


**Figure 18. GTTR accumulation rate during the rapid uptake phase.** The GTTR accumulation rate remained lowest in the magnesium-supplemented group even after onset of the rapid uptake phase.

The extent of accumulation, as measured by maximum mean Texas Red fluorescence, was consistent with the findings related to GTTR accumulation rates. The highest maximum mean fluorescence was observed in the colistin-treated group, while the lowest maximum mean fluorescence was observed in the magnesium-supplemented group (Figure 19).

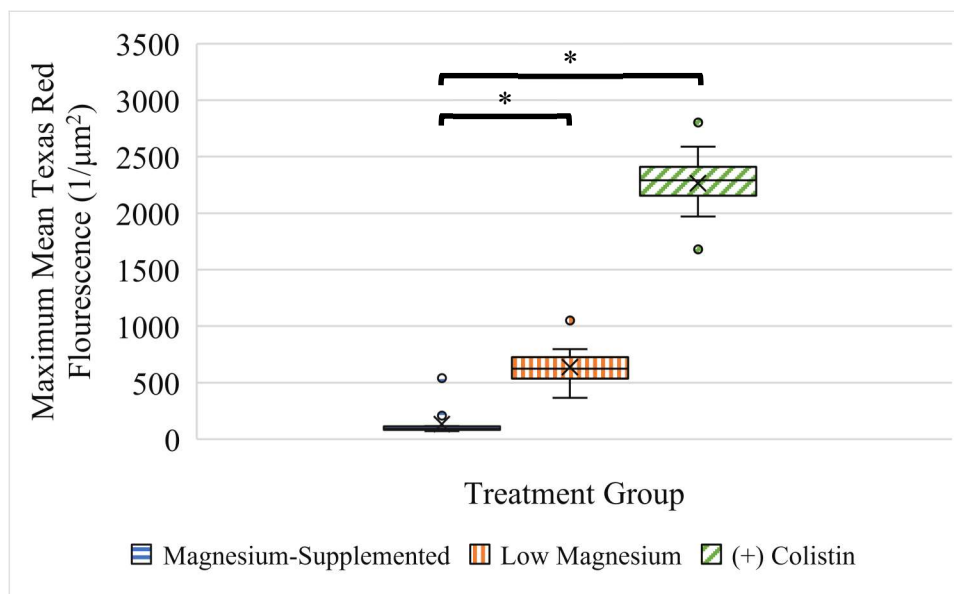


**Figure 19. Maximum mean Texas Red fluorescence observed over the course of gentamicin treatment.** Maximum Texas Red fluorescence values were lower for the magnesium-supplemented group than for either the low magnesium or colistin-treated group, indicating a greater extent of gentamicin accumulation in the latter two groups. This is consistent with what might be expected based on treatment-wise differences in membrane permeability.

Finally, to determine how differences in membrane stability influenced the timeline of gentamicin accumulation, the onset of the GTTR rapid uptake phase was measured. As expected, the onset of the GTTR rapid uptake phase occurred earlier in the colistin treatment group than it did for the magnesium-supplemented treatment group (Figure 20). Notably, there was not a significant difference in the onset of the GTTR rapid uptake phase observed between the magnesium-supplemented and low magnesium treatment groups.

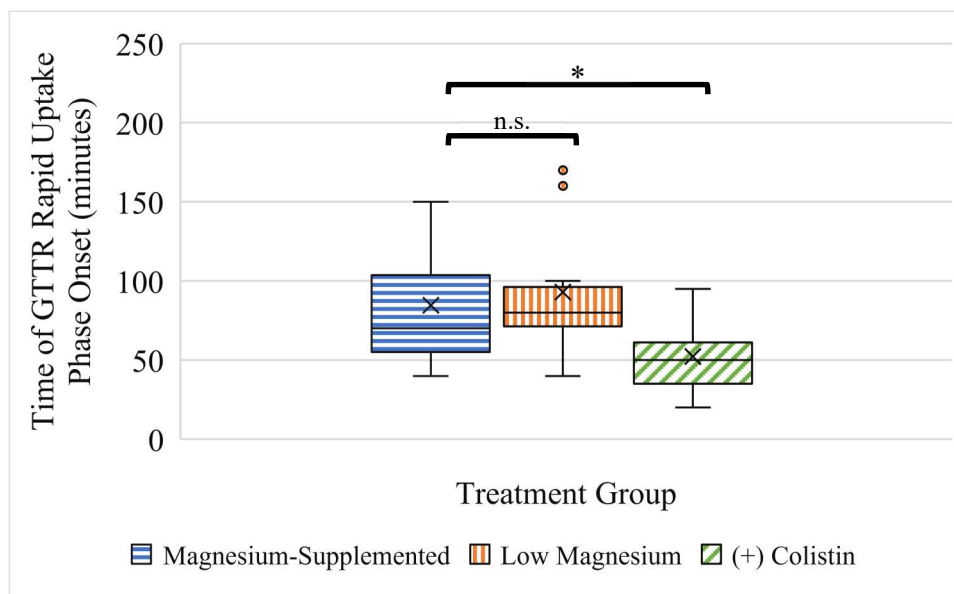


**Figure 20. Time of GTTR rapid uptake phase onset.** Onset of GTTR rapid uptake phase is hastened by colistin treatment.

In general, the GTTR accumulation results are consistent with what might be expected based on membrane permeability results. Given that the colistin-treated and low magnesium groups displayed increased membrane permeability relative to the magnesium-supplemented group across all SYTOX Green measures, increased permeability to gentamicin is expected. Indeed, GTTR accumulation rates were higher in the low magnesium and colistin-treated groups at both the early and later (during the GTTR rapid uptake phase) times. Furthermore, the extent of GTTR uptake was enhanced by colistin or low magnesium treatment, as evidenced by greater maximum mean Texas Red fluorescence values. Finally, the onset of the GTTR rapid uptake phase was hastened in the colistin treatment group, consistent with the earlier onset of the SYTOX Green rapid uptake phase. Altogether, increased membrane permeability appears to be associated with increased rates and extents of gentamicin uptake, as well as a shortened time scale over which this

occurs. All GTTR accumulation results discussed here are summarized quantitatively in Table 2 (Appendix B).

Additional evidence for this relationship lies in correlations between uptake rates and maximum fluorescence values of Texas Red and SYTOX Green. The rapid uptake phase accumulation rates of GTTR were positively correlated with the rapid uptake phase uptake rates of SYTOX Green. The strength of the correlation varied from moderate to high based on the treatment group, with the highest correlation observed in the magnesium-supplemented group (Figure 21).

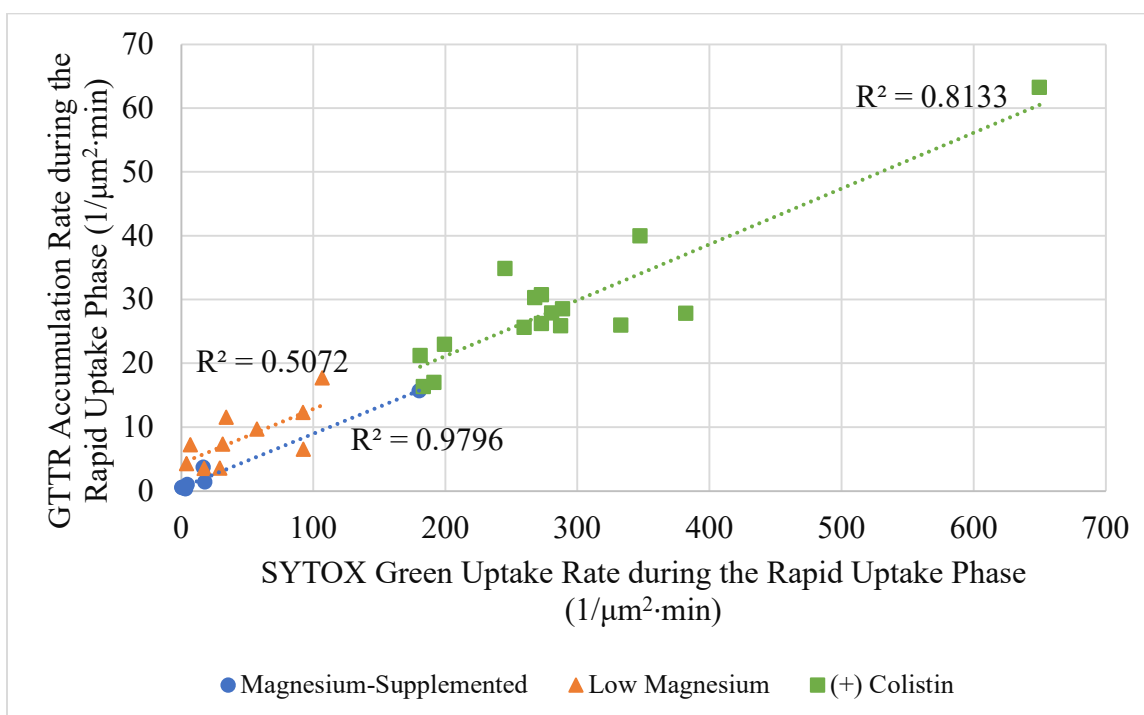


**Figure 21. Correlation between rapid uptake phase rates of GTTR accumulation and SYTOX Green uptake.** Positive correlations between rapid uptake phase uptake rates were observed in all treatment groups.

The same was true for correlations between maximum mean Texas Red fluorescence and maximum mean SYTOX Green fluorescence, although in this case, the low magnesium group showed the strongest correlation (Figure 22).

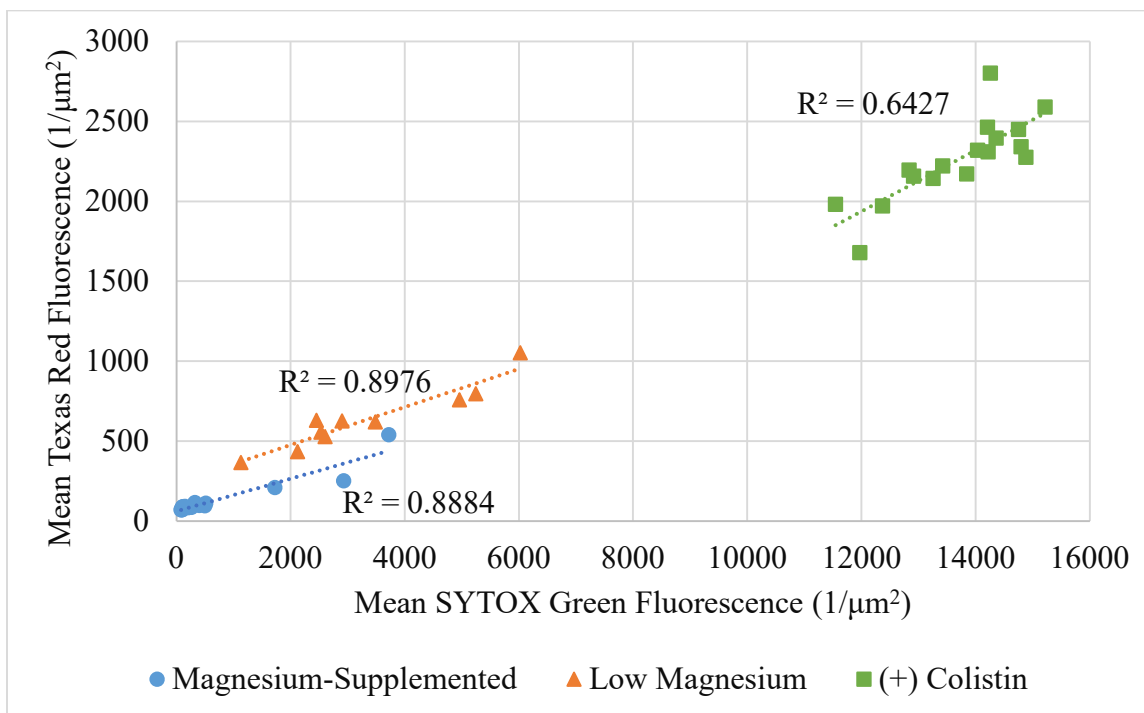


**Figure 22. Correlation between maximum mean Texas Red and SYTOX Green fluorescence.**

Positive correlations between maximum fluorescence values were observed in all treatment groups.

Taken together, these findings further support the observation that increased membrane permeability is associated with increased rates and extents of gentamicin accumulation.

## Measures of Growth and Growth Inhibition

Measurement of the exponential-phase growth rate constant and doubling time allowed for an assessment of colony growth, while determination of the time of transition from the exponential growth phase to the stationary phase ( $T_t$ ) and time of onset of stationary phase ( $T_s$ ) allowed for an assessment of the timeline of growth inhibition. There were not meaningful differences between treatment groups in either the exponential growth rate constant (Figure 23) or the doubling time (Figure 24).

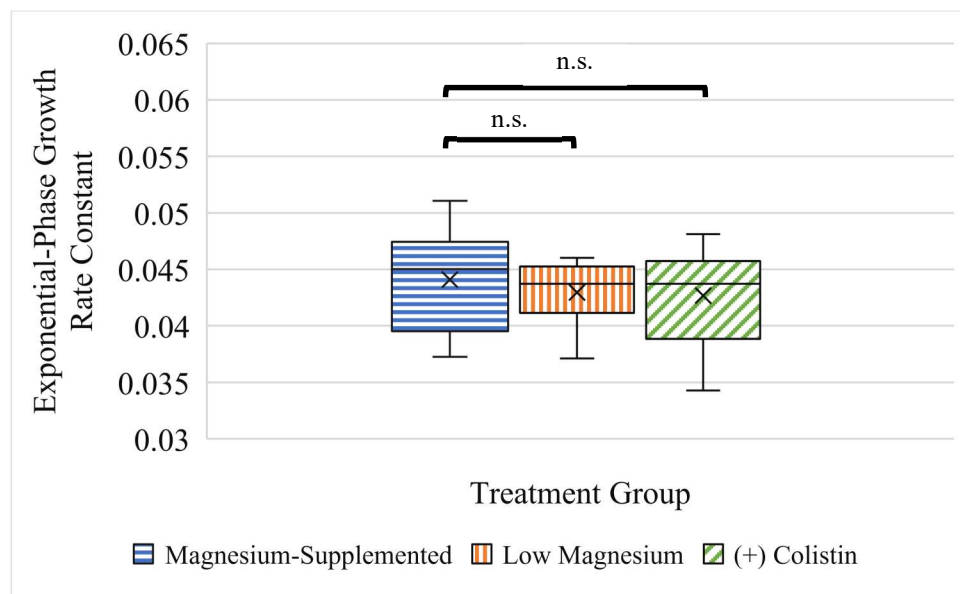


**Figure 23. Growth rate constant during the exponential phase.** The growth rate constant, a measure of colony growth during the exponential growth phase, did not vary by treatment.

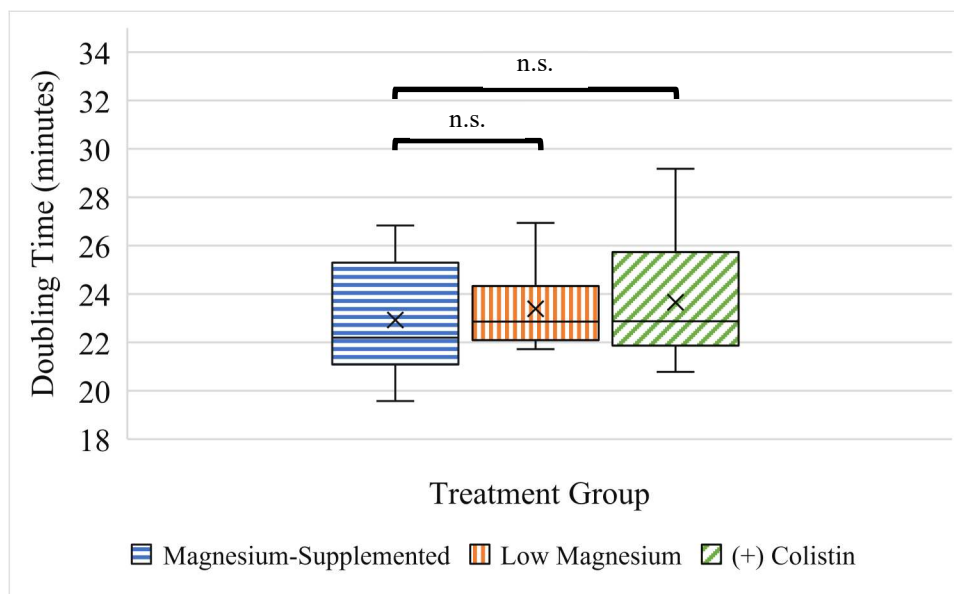


**Figure 24. Colony area doubling time.** The doubling time, an approximation of the time required for the population size to double, did not vary by treatment.

$T_t$  was used as an approximation for the time at which a colony transitioned from the exponential growth phase to the stationary phase, while  $T_s$  was the time after which colony growth ceased completely for all cells in the colony. While there appears to be similar trends in  $T_t$  (Figure 25) and  $T_s$  (Figure 26) on gross observation, statistical analysis shows that there were variations in trends between these two measures. While there were no significant differences in  $T_t$  between the magnesium-supplemented and other treatment groups, this was not the case for  $T_s$ , for which a statistically significant difference between the magnesium-supplemented and colistin-treated group was found.

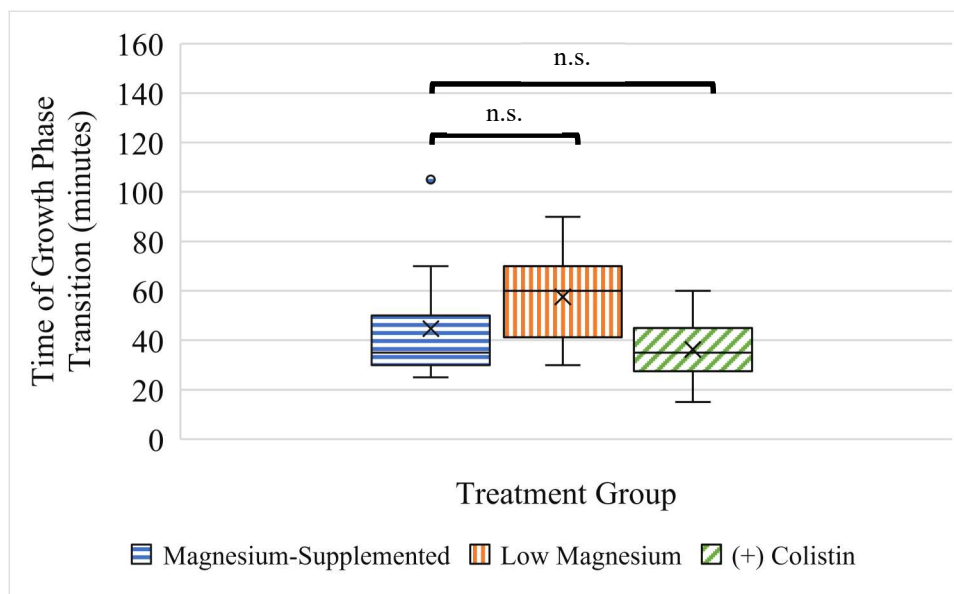


**Figure 25. Time of transition from the exponential growth phase to the stationary phase.**

There is no significant difference in  $T_t$  between treatment groups.

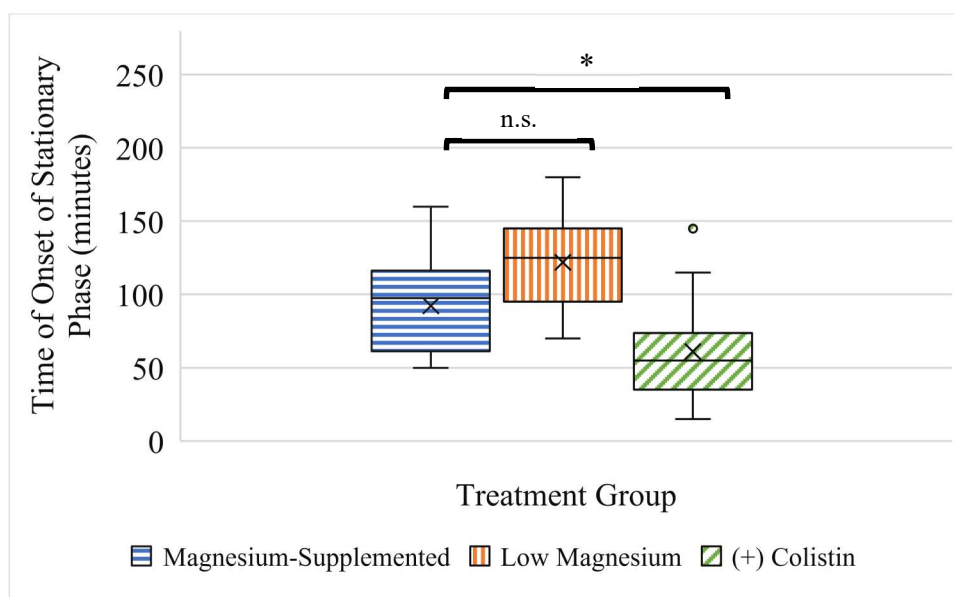


**Figure 26. Time of onset of the stationary phase.**  $T_s$  does not vary significantly between magnesium treatment groups but is significantly lower for the colistin-treated group than for the magnesium-supplemented group.

All growth and growth inhibition-related results discussed here are summarized in Table 3 (Appendix B).

### Relationships between Permeability, Accumulation, and Early Growth

The lack of significant differences in growth rate between treatment groups is particularly interesting in the context of the significant differences in gentamicin accumulation or membrane permeability observed during early experimental time points. To further explore this observation, we plotted exponential phase growth rate constant against initial SYTOX Green uptake rate, by colony, for each treatment group (Figures 27, 28, and 29). Note that each point in these plots represents a single colony within the treatment group.

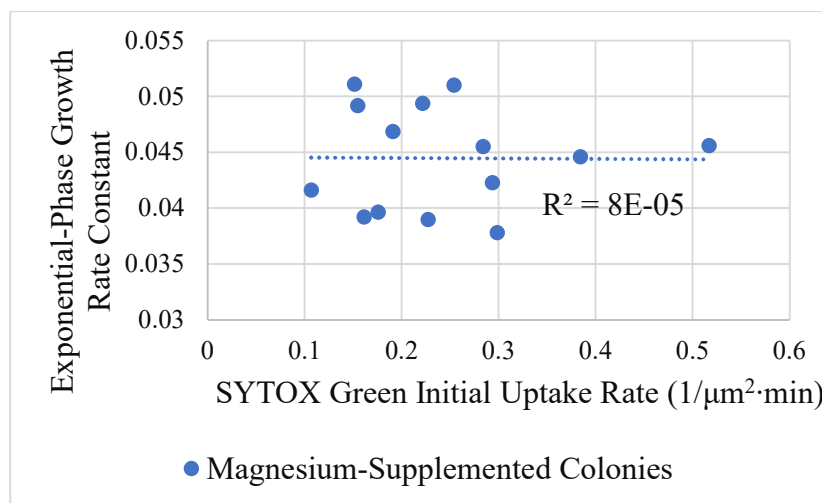


**Figure 27. Colony-level correlation between SYTOX Green initial uptake rate and exponential-phase growth rate constant, magnesium-supplemented colonies.** For magnesium-supplemented colonies, there is not a meaningful correlation between initial SYTOX Green uptake rate and exponential-phase growth rate constant ( $R^2 = 8\text{E}-05$ ).

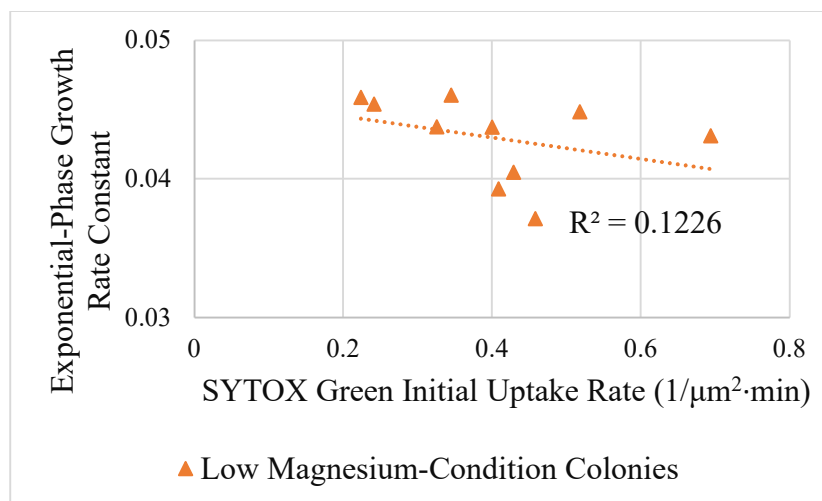


**Figure 28. Colony-level correlation between SYTOX Green initial uptake rate and exponential-phase growth rate constant, low magnesium-condition colonies.** For colonies cultured under relatively low magnesium conditions, there is minimal correlation between initial SYTOX Green uptake rate and exponential-phase growth rate constant ( $R^2 = 0.1226$ ).

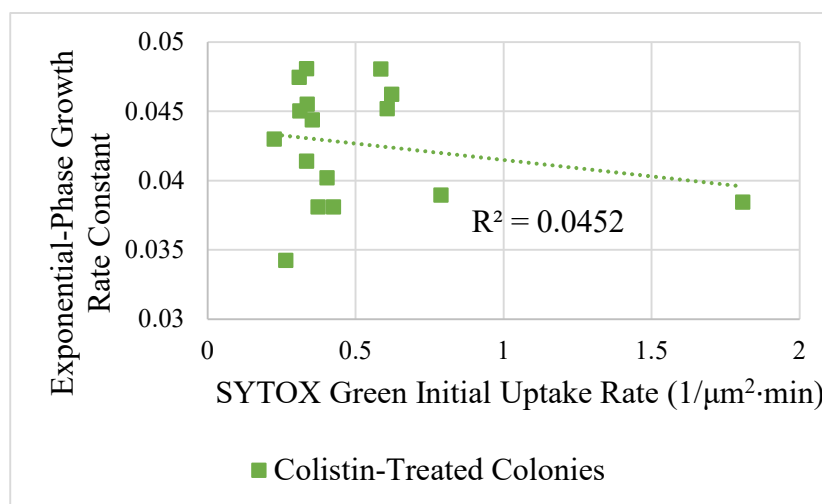


**Figure 29. Colony-level correlation between SYTOX Green initial uptake rate and exponential-phase growth rate constant, colistin-treated colonies.** For colonies treated with both gentamicin and colistin, there is minimal correlation between initial SYTOX Green uptake rate and exponential-phase growth rate constant ( $R^2 = 0.0452$ ).

Similar results were observed for the correlations between initial GTTR accumulation rate and exponential growth rate constant (Figures 30, 31, and 32).

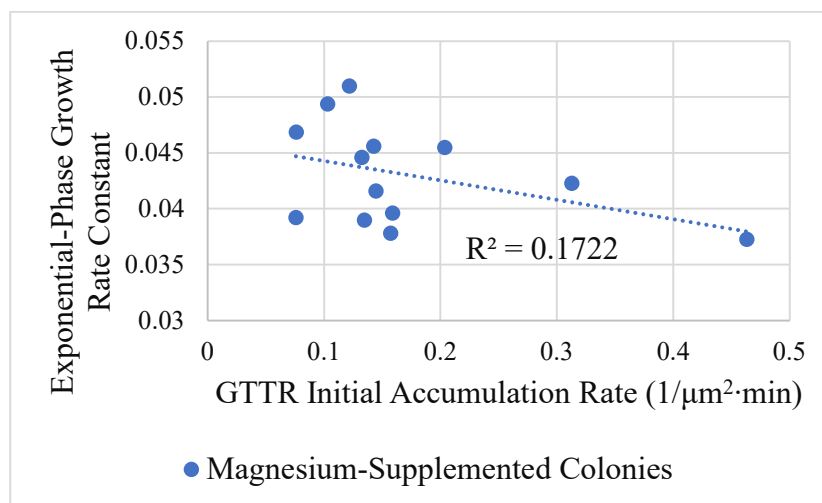


**Figure 30. Colony-level correlation between GTTR initial accumulation rate and exponential-phase growth rate constant, magnesium-supplemented colonies.** For magnesium-supplemented colonies, there is only a minimal correlation between GTTR initial accumulation rate and exponential-phase growth rate constant ( $R^2 = 0.1722$ ).

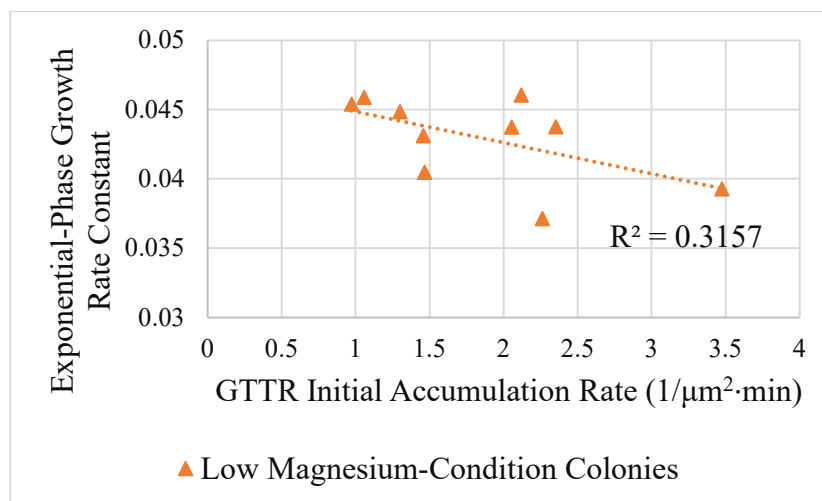


**Figure 31. Colony-level correlation between GTTR initial accumulation rate and exponential-phase growth rate constant, low magnesium-condition colonies.** For colonies cultured under relatively low magnesium conditions, there is only a weak correlation between GTTR initial accumulation rate and exponential-phase growth rate constant ( $R^2 = 0.3157$ ).

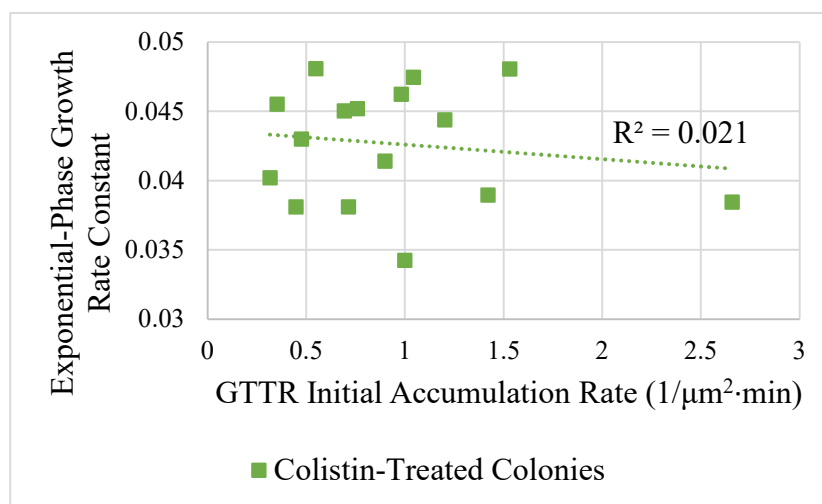


**Figure 32. Colony-level correlation between GTTR initial accumulation rate and exponential-phase growth rate constant, colistin-treated colonies.** For colonies treated with both gentamicin and colistin, there is minimal correlation between GTTR initial accumulation rate and exponential-phase growth rate constant ( $R^2 = 0.021$ ).

To summarize, minimal to weak correlations were observed between exponential-phase growth rate constant and either SYTOX Green initial uptake rate or GTTR initial accumulation rate. This was true across all treatment groups. While our earlier results indicated that significant differences to membrane permeability and gentamicin accumulation noted early in experimental observation were not reflected in growth rate during this time, it was unclear whether this same result would be true when considering individual colonies. We see here that this is indeed the case: colony-level variability in permeability or accumulation does not explain well the variability in initial growth rate. To understand whether these results are meaningful in the context of gentamicin mechanism of action, it is necessary to consider relationships between permeability, accumulation, and growth inhibition.

#### Relationships between Permeability, Accumulation, and Growth Inhibition

To assess the temporal relationships between events related to growth arrest, rapid changes in antibiotic accumulation, and the rapid onset of membrane permeabilization, the time from  $T_t$  and  $T_s$  to the onset of the SYTOX Green rapid uptake phase and the time from  $T_t$  and  $T_s$  to the onset the GTTR rapid uptake phase were measured.

The time from growth phase transition to the time of the SYTOX Green rapid uptake phase was found using the following calculation:

$$\textit{Time of SYTOX Green rapid uptake phase onset} - T_t$$

Positive values indicate that large losses in membrane integrity occurred after the time of growth phase transition, whereas negative values indicate the opposite order of events. A similar

calculation was performed to assess how the onset of the stationary phase was temporally related to large losses in membrane permeability:

$$\text{Time of SYTOX Green rapid uptake phase onset} - T_s$$

Both of these calculations were performed for each colony in each treatment group. The results are shown below (Figure 33 and Figure 34, respectively).

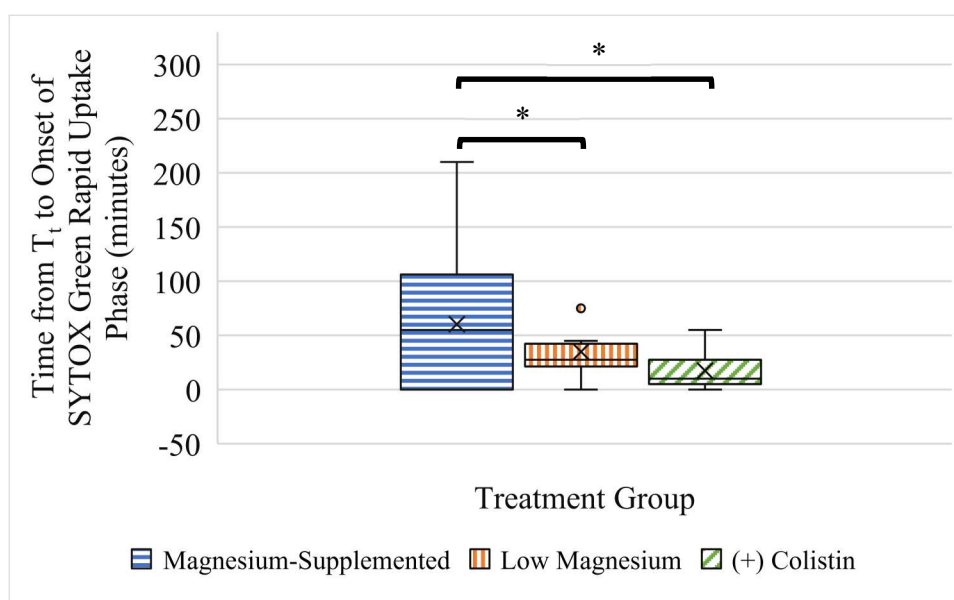


**Figure 33. Time from growth phase transition to onset of SYTOX Green rapid uptake phase.**

The time from the  $T_t$  to the onset of the SYTOX Green rapid uptake phase was always positive, indicating that, on average, cells experienced growth arrest before large losses in membrane integrity occurred.

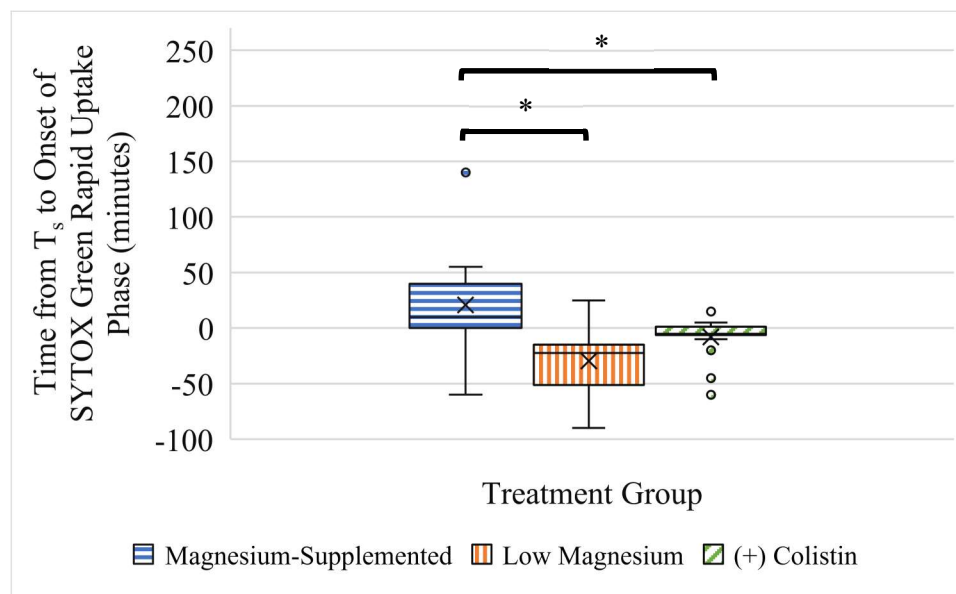


**Figure 34. Time from the onset of stationary phase to onset of SYTOX Green rapid uptake phase.** Given that there are both positive and negative values for this calculation observed in each treatment group, there is no consistent temporal relationship between the onset of the SYTOX Green rapid uptake phase and  $T_s$ . Within each treatment group, some colonies became completely growth-arrested before large losses in membrane integrity occurred, while large losses in membrane integrity preceded growth arrest of the last cell for other colonies.

Analogous calculations were performed to determine how the timeline of growth arrest related to the timeline of changes in antibiotic accumulation. The first calculation was performed to determine the time from  $T_t$  to the onset of the GTTR rapid uptake phase.

$$\text{Time of GTTR rapid uptake phase onset} - T_t$$

The second calculation was performed to determine the time from  $T_s$  to the onset of the GTTR rapid uptake phase.

*Time of GTTR rapid uptake phase onset –  $T_s$*

For each calculation, positive values indicate that the measure of growth arrest (either  $T_t$  or  $T_s$ ) occurred before large influxes of antibiotic occurred, as indicated by the onset of the GTTR rapid uptake phase. Negative values indicate that this increase in accumulation rate occurred prior to the measure of growth arrest. The results of these calculations are displayed below (Figure 35 and Figure 36, respectively).

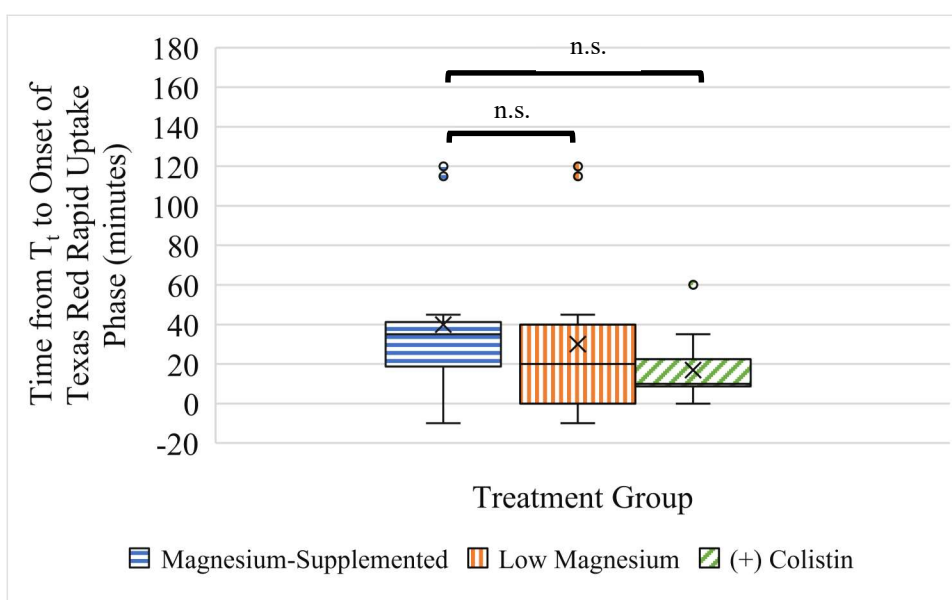


**Figure 35. Time from growth phase transition to onset of the GTTR rapid uptake phase.**

The presence of both positive and negative values in all treatment groups indicates that there is no consistent temporal relationship between the time of growth phase transition and the time at which gentamicin accumulation rates rapidly increase.

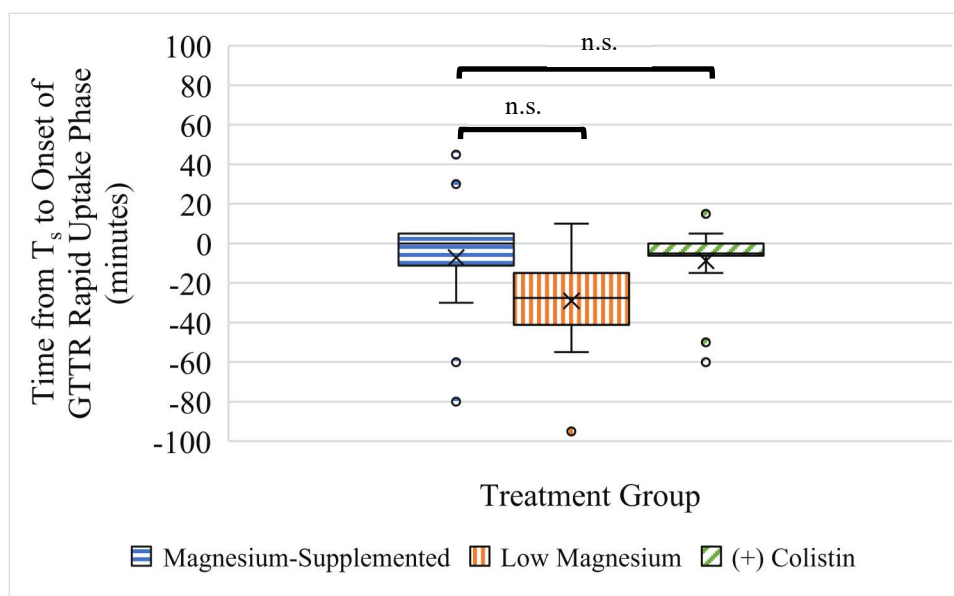


**Figure 36. Time from the onset of stationary phase to onset of GTTR rapid uptake phase.**

All colonies show both positive and negative values within their distributions for this time difference. Given this, there is no clear temporal relationship observed between the onset of the stationary phase and large increases in gentamicin accumulation rate.

To summarize, there were no clear temporal relationships found between the onset of the GTTR rapid accumulation phase and either measure of growth arrest, or between the onset of the SYTOX Green rapid accumulation phase and the onset of the stationary phase. These results suggest that large losses in membrane integrity, or large influxes of antibiotic, are not required to initiate growth arrest. While a consistent temporal trend was observed when comparing  $T_t$  and the onset of the SYTOX Green uptake phase, the relationship was that growth phase transition always occurred prior to large losses in membrane integrity. This indicates that, on average, cells became growth arrested prior to significant changes in membrane integrity. Like the other results presented in this section, this suggests that membrane permeabilization is not a prerequisite to the initiation

of growth arrest. The results reported in this section are summarized quantitatively in Table 4 (Appendix B.)

To determine whether there were trends in the extents of GTTR accumulation or membrane permeabilization at the onset of the stationary phase, the mean Texas Red fluorescence and mean SYTOX Green fluorescence values at  $T_s$  were collected. Given that the onset of the stationary phase is indicative of the first time at which all cells in the colony are growth-arrested, we are interested in determining whether there is a threshold amount of antibiotic accumulation or membrane permeability required to halt all cell growth.

Our results show that there were clear differences in mean Texas Red fluorescence values at  $T_s$  observed between treatment groups (Figure 37), indicating that there is not a threshold amount of gentamicin accumulation required to initiate growth arrest of all cells regardless of treatment.

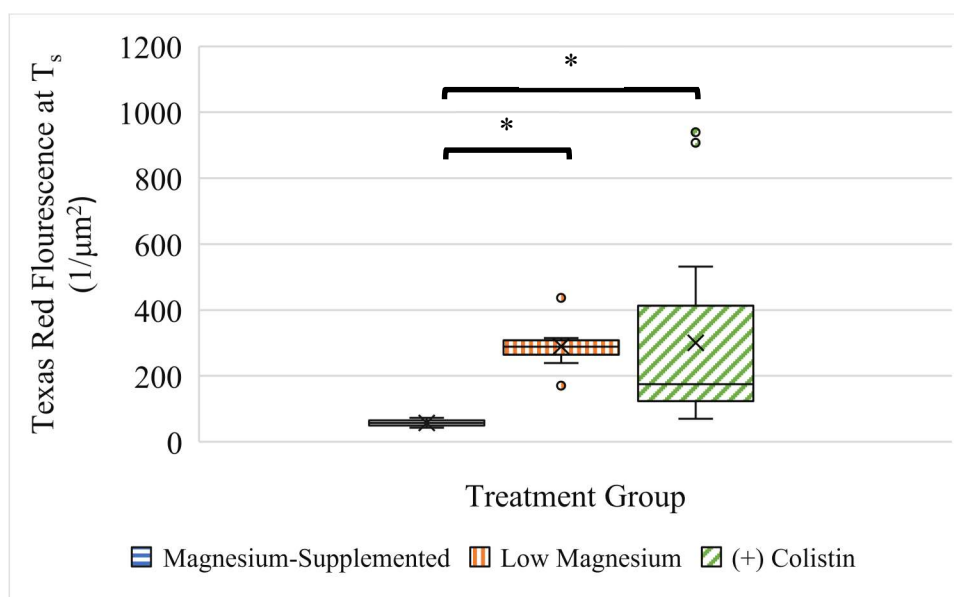


**Figure 37. Mean Texas Red fluorescence at the time of stationary phase onset.** There are significant differences in GTTR accumulation at the time of colony growth arrest.

Differences in SYTOX Green fluorescence values at  $T_s$  were also observed (Figure 38). Similar to the measures of Texas Red fluorescence at  $T_s$ , these results indicate that there is not a threshold amount of membrane damage required to initiate growth arrest of all cells regardless of treatment.

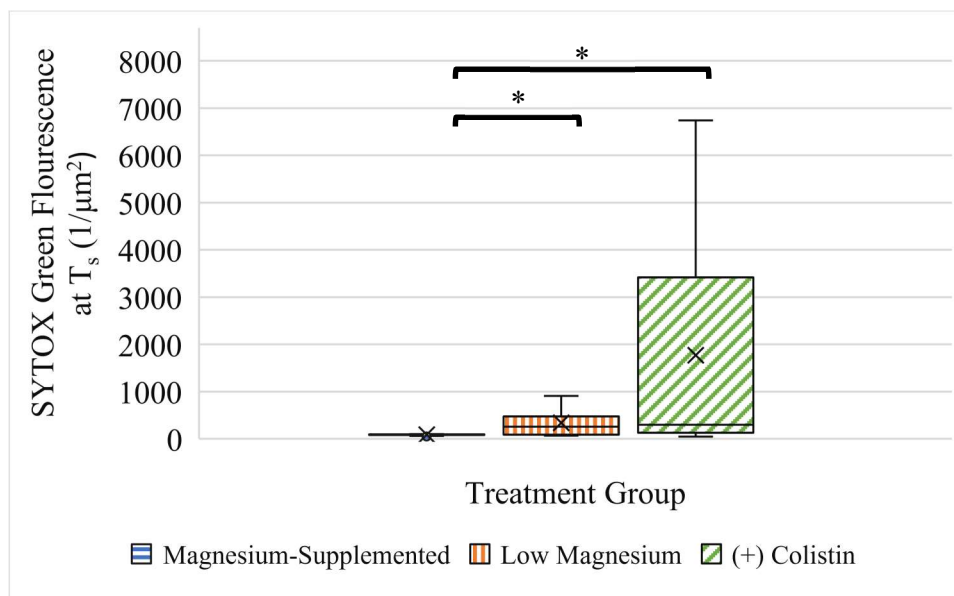


**Figure 38. Mean SYTOX Green fluorescence at the time of stationary phase onset.** The extent of membrane damage at  $T_s$  varies significantly by treatment.

These results are summarized quantitatively in Table 5 (Appendix B). Taken together, these findings indicate that there is not a consistent threshold level of membrane damage or antibiotic accumulation required to initiate growth arrest of all cells in a given colony. However, it is worth noting the influence of the discrete nature of the time points used to determine  $T_s$ . Given that each time point was separated by five minutes, it is possible that there is not enough precision in the measurements of  $T_s$  to determine whether fluorescence values at the exact time of growth arrest vary meaningfully across colonies. Furthermore, both measures of fluorescence and growth

are representative of the entire colony data, so study at the single cell level may produce more meaningful results.

## CHAPTER V

### DISCUSSION

#### Summary and Implications

At present, there exists in the literature a number of conflicting hypotheses implicating the role of membrane damage in aminoglycoside mechanism of action. In this study, we examined the relationship between cell growth and growth inhibition, antibiotic accumulation, and membrane permeability changes in *Escherichia coli* microcolonies during treatment with an aminoglycoside antibiotic, gentamicin, to assess whether a causal link between membrane damage and subsequent growth arrest could be supported.

Relative reductions in membrane integrity induced by low magnesium conditions or treatment with colistin were observed across multiple measures related to membrane permeability. Initial and rapid uptake phase SYTOX Green uptake rates, maximum SYTOX Green fluorescence, and onset of the SYTOX Green rapid uptake phase indicated that membrane permeabilization occurred earlier and to greater extents in the low magnesium and colistin treatment groups, consistent with our expectations that these treatments would result in decreased membrane integrity relative to the magnesium-supplemented group. The effects of increased membrane permeability on gentamicin accumulation were also consistent with our expectations, with greater

initial and rapid uptake phase GTTR accumulation rates, as well as greater maximum Texas Red fluorescence, observed in treatment groups showing increased membrane permeability in the SYTOX Green studies. Correlations between Texas Red and SYTOX Green rapid uptake phase uptake rates and maximum fluorescence values offer further evidence for this relationship. Taken together, these results support the claims that, in the context of gentamicin treatment, (1) increased magnesium availability improves membrane stability, (2) treatment with colistin reduces membrane stability, and (3) reductions in membrane stability increase gentamicin accumulation.

These results are consistent with our expectations based on the existing literature. However, what is particularly interesting about these results is that changes in membrane stability and gentamicin accumulation do not result in significant changes to a number of growth-related parameters. Measurements of the exponential phase growth rate constant, doubling time, and time of growth phase transition did not vary significantly between groups. This is notable for two reasons. The first is that, despite evidence that there are significant differences in membrane permeability and gentamicin accumulation observed between groups during the early time points of observation, there were no significant consequences to growth during this period. This was reflected in the correlations between initial SYTOX Green and GTTR uptake rates and exponential-phase growth rate constant observed when these relationships were examined at the colony level. The second is that the onset of growth arrest did not correlate with differences in these conditions, with no significant differences between groups observed in the time of growth phase transition. While the time of onset of the stationary phase did differ between the magnesium-supplemented and colistin-treated groups, this difference did not exist between magnesium treatments, suggesting that membrane damage alone is not the causal agent of growth inhibition. Furthermore, our findings related to the extent of SYTOX Green uptake at the onset of the

stationary phase indicate that there is no observable degree of membrane damage required to halt colony growth. Ultimately, our results indicate that higher initial rates of gentamicin accumulation and membrane permeability fail to reliably predict corresponding reductions in growth rate or time to growth arrest. Implications of this finding include the possibility that only small amounts of gentamicin may be required to initiate the onset of growth arrest.

Support for the claim that membrane damage is not the causal agent of growth inhibition is also found in our results related to the timeline of gentamicin activity. For all colonies in all treatment groups, the time of growth phase transition occurred before the SYTOX Green rapid uptake phase, indicating that large losses in membrane integrity are not required for the initiation of growth inhibition. Furthermore, there was no clear temporal relationship between the time of onset of the stationary phase and time of onset of the SYTOX Green rapid uptake phase, with these events occurring in either sequence depending on colony. The same was true for the onset of the GTTR rapid uptake phase, although whether this phase is the result of membrane permeabilization or changes in cell physiology is unclear. Regardless, the timeline of membrane damage does not correlate well with that of growth arrest.

In the context of existing models, findings of this study fail to support the role of membrane damage as the primary harbinger of growth inhibition. While membrane damage is certainly important in hastening this process, it in itself is likely not the central catalyst for the initiation of growth arrest. This would explain why larger initial rates of gentamicin accumulation seen in the low magnesium treatment group do not correlate with changes to the growth inhibition timeline compared to the that of the magnesium-supplemented group. While lower local magnesium concentrations might accelerate the process of gentamicin adsorption to the outer membrane, the fact that there is little effect on the integrity of the inner membrane would result in similar timelines

of growth inhibition between magnesium treatment groups. This makes sense in the context of prior studies of aminoglycoside uptake, which indicate that initial antibiotic accumulation after the adsorption phase occurs in a slow, energy-dependent manner after the initial adsorption phase (Krause et. al., 2016). Unfortunately, our study is limited insofar as it was not possible to distinguish between gentamicin adsorption, entry into the periplasmic space, and ultimate accumulation in the cytoplasm, the site of ribosome inactivation. However, this possible explanation would be consistent with the colistin-group findings for onset of stationary phase, which occurred significantly earlier than did the onset of stationary phase for the magnesium-supplemented group. Since colistin initiates damage to both the outer membrane and inner membrane, the timeline of gentamicin accumulation and subsequent ribosome inactivation is accelerated, resulting in an earlier onset of growth arrest. While at present these suggestions are limited to speculation, they are consistent with the known concentration dependence of aminoglycoside activity (Levison and Levison, 2009). Furthermore, they do not invalidate the long-standing observation that the bactericidal action of gentamicin is dependent on its accumulation (Heller et. al., 1980). Nonetheless, further study is critical to understanding the true course of events occurring over the timescale of gentamicin activity.

### Future Directions

Given the results and limitations of this study, there are a number of ways in which aminoglycoside mechanism of action might be clarified through future work. First, the construction of an accurate timeline of inhibition, accumulation, and changes to membrane permeability requires investigation at the single cell level. While this study has been useful in describing general relationships between these processes, it is not possible to predict the trends

that may emerge with improved resolution as it pertains to individual cell physiology. For example, our analysis related to the extents of Texas Red and SYTOX Green fluorescence at the times of growth phase transition and onset of the stationary phase are limited insofar as we are considering the mean fluorescence values across all pixels for the entire colony. This inherently limits the conclusions we are able to draw regarding the precise relationships between accumulation, permeability, and growth arrest. Furthermore, analysis at the cellular level would ideally allow for a better mathematical characterization of antibiotic accumulation and SYTOX Green uptake kinetics. At present, our ability to analyze these trajectories is limited by the confounding effects of observing what is essentially an average of many single cells. It was necessary to make mathematical assumptions to account for variation between colonies, which may or may not have been consistent with the underlying biological processes being observed. While significant variation between individual trajectories would almost certainly remain, single cell studies would reduce the simplifications necessary to make meaningful comparisons between groups during data analysis. Furthermore, trends in the data would better reflect biological reality, and variability could be more clearly attributed to physiological differences between individuals. Ideally, this would also result in the ability to use mathematical models that prevent the need to exclude any data from analysis.

Increased sensitivity of the accumulation and permeability probes is also likely to improve the clarity of these findings. While clear spikes in Texas Red and SYTOX Green were observable, there may be more subtle changes in accumulation dynamics and permeability changes that could prove to be important in characterizing the sequence of events occurring in cells during aminoglycoside treatment. There may also be significant findings related to the spatial distribution of antibiotic uptake. At present, it is not possible to distinguish between the processes of adsorption

to the outer membrane, passage through the inner and outer membranes, or the location of ribosome binding, either in the cytoplasm or at membrane-bound ribosomes. Increased sensitivity of fluorescent probes may allow for improved resolution in terms of visualizing these processes in the data.

Alone or in addition to these changes, the ability to distinguish between growth inhibition and death would be a significant improvement to our study. Although gentamicin is considered a bactericidal antibiotic (Gonzalez and Spencer, 1998), we cannot make the assumption that the growth inhibition observed here was indicative of a concurrent process of cell death. Clarification of the timeline of bactericidal activity would provide the context necessary to draw stronger conclusions regarding the precise mechanism of action of gentamicin and, in doing so, more clearly describe the antibiotic behavior of aminoglycosides.

## APPENDIX A

### COLONY DATA IN THE CONTEXT OF CELL HETEROGENEITY

Despite variability in the time-course trajectories of gentamicin accumulation, SYTOX Green uptake, and precise patterns of growth observed between individual cells within a given colony, our single-cell findings indicate that measurements of these trajectories taken at the colony level were appropriate for the purposes of this study. When single cell length measurements were compared against the colony data, we found that variation in the time of growth arrest for single cells corresponded to the period of transition from the exponential to stationary growth phase, as observed in the colony growth trajectories (Figure 39). The implication of this is that colony-level measurement for time of growth phase transition ( $T_t$ ) corresponds roughly to a midpoint in the distribution of individual cell growth arrest, while colony-level time of stationary phase onset ( $T_s$ ) corresponds to the last time of growth arrest amongst single cells of that colony. Given these relationships, the colony-level parameters were good approximations for the corresponding events at the single cell level.

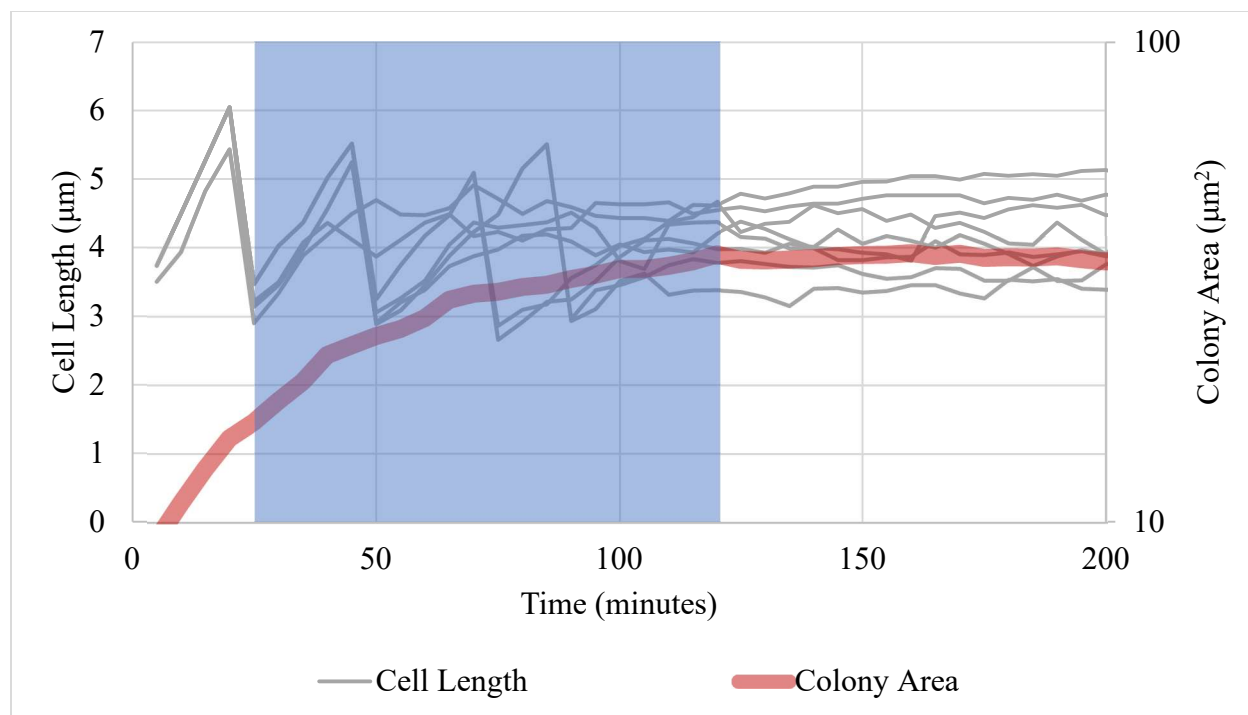


**Figure 39. Relationship between cell and colony growth arrest.** Here, cell length trajectories for individual cells are shown in grey, while total colony area is shown in pink. Sharp declines in cell length mark the occurrence of a cell division. Some cells become growth-arrested shortly after the first division, while others divide up to three times before becoming growth-arrested. The transitional period over which colony growth transitions from the exponential to stationary phase (blue) corresponds to variable onsets of growth arrest of individual cells in the colony.

In terms of the SYTOX Green trajectories, we found that analysis of colony-level data was also appropriate for our purposes. The primary difference between these and the comparison of colony and single-cell growth metrics was that these trajectories were more dependent on individual cells as opposed to reflective of all cells equally. When analyzing single-cell data, we found that the SYTOX Green rate spikes observed at the colony level were, at least in the initial time points of that phase, the result of a single cell suddenly losing membrane integrity. The

fluorescence during this event was so great that the colony-level SYTOX Green trajectory became essentially a reflection of that occurring for the single cell. A linear regression performed to compare the colony and single cell's SYTOX Green uptake trajectories showed that the two were highly correlated ( $R^2 = 0.943$ ). While several of the other cells exhibited their own rapid uptake phases later in the time series, the effect on the colony-level data was not as extreme due to the high SYTOX fluorescence already present. In general, the higher the maximum fluorescence value observed for a single cell, the higher the correlation observed between the SYTOX Green fluorescence trajectories of that cell and the colony. A similar result was observed for the Texas Red fluorescence trajectories, although this trend in single cell-to-colony correlations was not as pronounced.

To summarize, the times of GTTR and SYTOX Green rapid uptake phase onsets observed at the colony level were equivalent to corresponding metrics of the first single cell in the colony to undergo these transitions. While future studies are necessary to improve the clarity of our assessments of the relationships between growth, accumulation, and permeability, preliminary findings at the single-cell level do not disagree with the overall conclusions of this study.

**APPENDIX B**  
**DATA TABLES**

**Table 1. Summary of SYTOX Green Uptake Parameters by Treatment**

SYTOX Green Uptake Parameter	Mean	Standard Deviation	N
<b>Initial Uptake Rate (<math>\mu\text{m}^2 \cdot \text{min}^{-1}</math>)</b>			
Magnesium-Supplemented	0.2	0.1	14
Low Magnesium	0.4	0.1	10
(+) Colistin	0.5	0.4	16
<b>Rapid Uptake Phase Uptake Rate (<math>\mu\text{m}^2 \cdot \text{min}^{-1}</math>)</b>			
Magnesium-Supplemented	21.5	53.0	11
Low Magnesium	47.2	37.8	10
(+) Colistin	290.1	112.1	16
<b>Maximum Mean Fluorescence (<math>\mu\text{m}^2</math>)</b>			
Magnesium-Supplemented	707.8	1106.9	16
Low Magnesium	3347.3	1563.7	10
(+) Colistin	13754.8	1084.7	16
<b>Time of Rapid Uptake Phase Onset (min)</b>			
Magnesium-Supplemented	134.5	57.3	11
Low Magnesium	92.5	28.2	10
(+) Colistin	52.8	24.2	16

**Table 2. Summary of Gentamicin-Texas Red Uptake Parameters by Treatment**

Gentamicin-Texas Red Uptake Parameter	Mean	Standard Deviation	N
<b>Initial Accumulation Rate (<math>\mu\text{m}^{-2}\cdot\text{min}^{-1}</math>)</b>			
Magnesium-Supplemented	0.2	0.1	13
Low Magnesium	1.9	0.8	10
(+) Colistin	0.9	0.6	16
<b>Rapid Uptake Phase Accumulation Rate (<math>\mu\text{m}^{-2}\cdot\text{min}^{-1}</math>)</b>			
Magnesium-Supplemented	2.2	4.4	12
Low Magnesium	8.4	4.5	10
(+) Colistin	29.1	10.9	16
<b>Maximum Mean Fluorescence (<math>\mu\text{m}^{-2}</math>)</b>			
Magnesium-Supplemented	134.4	119.5	16
Low Magnesium	637.1	195.9	10
(+) Colistin	2266.3	263.4	16
<b>Time of Rapid Uptake Phase Onset (min)</b>			
Magnesium-Supplemented	84.6	40.6	12
Low Magnesium	93.0	40.9	10
(+) Colistin	52.2	23.2	16

**Table 3. Summary of Growth Parameters by Treatment**

Growth Parameter	Mean	Standard Deviation	N
Exponential Growth Rate Constant ( $\text{min}^{-1}$ )			
Magnesium-Supplemented	0.044	0.005	16
Low Magnesium	0.043	0.003	10
(+) Colistin	0.043	0.004	16
Doubling Time (min)			
Magnesium-Supplemented	22.9	2.5	16
Low Magnesium	23.4	1.8	10
(+) Colistin	23.7	2.5	16
Time of Growth Phase Transition, $T_t$ (min)			
Magnesium-Supplemented	44.7	20.9	16
Low Magnesium	57.5	19.6	10
(+) Colistin	36.3	12.6	15
Time of Stationary Phase Onset, $T_s$ (min)			
Magnesium-Supplemented	92.2	34.8	16
Low Magnesium	122.0	37.7	10
(+) Colistin	60.9	34.4	16

**Table 4. Summary of Temporal Relationships Between Growth Arrest, Accumulation, and Permeability Changes by Treatment**

Calculation	Mean	Standard Deviation	N
Time from Growth Phase Transition to GTTR Rapid Uptake Phase (min)			
Magnesium-Supplemented	40.0	39.7	12
Low Magnesium	35.5	36.4	10
(+) Colistin	18.0	15.8	15
Time from Growth Phase Transition to SYTOX Green Rapid Uptake Phase (min)			
Magnesium-Supplemented	87.7	54.4	11
Low Magnesium	35.0	25.4	10
(+) Colistin	18.7	16.4	15
Time from Stationary Phase Onset to GTTR Rapid Uptake Phase (min)			
Magnesium-Supplemented	-9.6	34.6	12
Low Magnesium	-29.0	31.2	10
(+) Colistin	-8.8	19.3	16
Time from Stationary Phase Onset to SYTOX Green Rapid Uptake Phase (min)			
Magnesium-Supplemented	30.5	50.3	11
Low Magnesium	-29.5	34.4	10
(+) Colistin	-8.1	19.1	16

**Table 5. Mean Texas Red and SYTOX Green Fluorescence at T<sub>s</sub>**

Measurement	Mean	Standard Deviation	N
Mean Texas Red Fluorescence at T <sub>s</sub> (1/μm <sup>2</sup> )			
Magnesium-Supplemented	56.5	10.8	16
Low Magnesium	289.2	67.4	10
(+) Colistin	300.2	278.2	16
Mean SYTOX Green Fluorescence at T <sub>s</sub> (1/μm <sup>2</sup> )			
Magnesium-Supplemented	91.1	31.8	16
Low Magnesium	342.0	294.1	10
(+) Colistin	1768.2	2440.3	16

## REFERENCES

- Allen, R. J., & Waclaw, B. (2019). Bacterial growth: A statistical physicist's guide. *Reports on Progress in Physics*, 82(1). <https://doi.org/10.1088/1361-6633/aae546>
- Anand, N., Davis, B. D., & Armitage, A. K. (1960). Uptake of streptomycin by *Escherichia coli*. *Nature*, 185, 23–24. <https://doi.org/10.1038/185023a0>
- Andrade, F. F., Silva, D., Rodrigues, A., & Pina-Vaz, C. (2020). Colistin update on its mechanism of action and resistance, present and future challenges. *Microorganisms*, 8(11), 1716. <https://doi.org/10.3390/microorganisms8111716>
- Awodele, O., Tomoye, O. P., Quashie, N. B., Amagon, K. I., & Ogunnowo, S. A. (2015). Gentamicin nephrotoxicity: Animal experimental correlate with human pharmacovigilance outcome. *Biomedical Journal*, 38(2), 125–130. <https://doi.org/10.4103/2319-4170.131387>
- Bader, M. S., Loeb, M., & Brooks, A. A. (2017). An update on the management of urinary tract infections in the era of antimicrobial resistance. *Postgraduate Medicine*, 129(2), 242–258. <https://doi.org/10.1080/00325481.2017.1246055>
- Bozkurt-Güzel, C., & Gerçeker, A. A. (2012). Post-antibiotic effect of colistin, alone and in combination with amikacin, on *Pseudomonas aeruginosa* strains isolated from cystic fibrosis patients. *The Journal of Antibiotics*, 65(2), 83–86. <https://doi.org/10.1038/ja.2011.101>

- Brook, I., & Walker, R. I. (1985). Interaction between penicillin, clindamycin or metronidazole and gentamicin against species of *Clostridia* and anaerobic and facultatively anaerobic Gram-positive cocci. *The Journal of Antimicrobial Chemotherapy*, *15*(1), 31–37.  
<https://doi.org/10.1093/jac/15.1.31>
- Bryan, L. E., & Kwan, S. (1983). Roles of ribosomal binding, membrane potential, and electron transport in bacterial uptake of streptomycin and gentamicin. *Antimicrobial Agents and Chemotherapy*, *23*(6), 835–845. <https://doi.org/10.1128/aac.23.6.835>
- Chen, C., Chen, Y., Wu, P., & Chen, B. (2014). Update on new medicinal applications of gentamicin: Evidence-based review. *Journal of the Formosan Medical Association*, *113*(2), 72–82. <https://doi.org/10.1016/j.jfma.2013.10.002>
- Davis, B. D. (1987). Mechanism of bactericidal action of aminoglycosides. *Microbiological Reviews*, *51*(3), 341–350. <https://www.ncbi.nlm.nih.gov/pmc/articles/PMC373115/>
- Davis, B. D., Chen, L. L., & Tai, P. C. (1986). Misread protein creates membrane channels: An essential step in the bactericidal action of aminoglycosides. *Proceedings of the National Academy of Sciences of the United States of America*, *83*(16), 6164–6168.  
<https://doi.org/10.1073/pnas.83.16.6164>
- Follenius-Wund, A., Bourotte, M., Schmitt, M., Iyice, F., Lami, H., Bourguignon, J. J., Haiech, J., & Pigault, C. (2003). Fluorescent derivatives of the GFP chromophore give a new insight into the GFP fluorescence process. *Biophysical Journal*, *85*(3), 1839–1850.  
[https://doi.org/10.1016/S0006-3495\(03\)74612-8](https://doi.org/10.1016/S0006-3495(03)74612-8)

- Fourmy, D., Recht, M., Blanchard, S., & Puglisi, J. (1996). Structure of the A site of *Escherichia coli* 16S ribosomal RNA complexed with an aminoglycoside antibiotic. *Science*, 274(5291), 1367-1371. <http://www.jstor.org/stable/2892058>
- Freeman, C. D., Nicolau, D. P., Belliveau, P. P., & Nightingale, C. H. (1997). Once-daily dosing of aminoglycosides: Review and recommendations for clinical practice. *The Journal of Antimicrobial Chemotherapy*, 39(6), 677–686. <https://doi.org/10.1093/jac/39.6.677>
- Gary, N. E., Buzzeo, L., Salaki, J., & Eisinger, R. P. (1976). Gentamicin-associated acute renal failure. *Archives of internal medicine*, 136(10), 1101–1104. <https://pubmed.ncbi.nlm.nih.gov/788666/>
- Geladari, A., Simitsopoulou, M., Antachopoulos, C., & Roilides, E. (2019). Dose-dependent synergistic interactions of colistin with rifampin, meropenem, and tigecycline against carbapenem-resistant *Klebsiella pneumoniae* biofilms. *Antimicrobial Agents and Chemotherapy*, 63(3). <https://doi.org/10.1128/AAC.02357-18>
- Germovsek, E., Barker, C. I., & Sharland, M. (2017). What do I need to know about aminoglycoside antibiotics?. *Archives of Disease in Childhood - Education and Practice Edition*, 102(2), 89–93. <https://doi.org/10.1136/archdischild-2015-309069>
- Gonzalez, L. S., III, & Spencer, J. P. (1998). Aminoglycosides: A practical review. *American Family Physician*, 58(8), 1811–1820. <https://www.aafp.org/afp/1998/1115/p1811.html>
- Hancock, R. E. (1984). Alterations in outer membrane permeability. *Annual Review of Microbiology*, 38, 237–264. <https://doi.org/10.1146/annurev.mi.38.100184.001321>

- Heller, A. H., Spector, R., & Aalyson, M. (1980). Effect of sodium chloride on gentamicin accumulation by *Escherichia coli*: Correlation with bacterial growth and viability. *The Journal of Antibiotics*, 33(6), 604–613. <https://doi.org/10.7164/antibiotics.33.604>
- Inoue, K., Hattori, Y., Horie, M., Tomoaki Hino, & Oka, H. (2011). Preparative purification of gentamicin components using high-speed counter-current chromatography coupled with electrospray mass spectrometry. *Journal of Separation Science*, 34(12), 1484-1488. <https://doi-org.proxy.library.emory.edu/10.1002/jssc.201100114>
- Invitrogen. (n.d.). *SYTOX™ Green nucleic acid stain - 5 mM solution in DMSO*. ThermoFisher Scientific. <https://www.thermofisher.com/order/catalog/product/S7020#/S7020>
- Kapuscinski, J. (1995). DAPI: A DNA-specific fluorescent probe. *Biotechnic & Histochemistry : Official Publication of the Biological Stain Commission*, 70(5), 220–233. <https://doi.org/10.3109/10520299509108199>
- Kohanski, M. A., Dwyer, D. J., Wierzbowski, J., Cottarel, G., & Collins, J. J. (2008). Mistranslation of membrane proteins and two-component system activation trigger antibiotic-mediated cell death. *Cell*, 135(4), 679–690. <https://doi.org/10.1016/j.cell.2008.09.038>
- Kolozsvari, B., Parisi, F., & Saiardi, A. (2014). Inositol phosphates induce DAPI fluorescence shift. *The Biochemical Journal*, 460(3), 377–385. <https://doi.org/10.1042/BJ20140237>

- Kotra, L. P., Haddad, J., & Mobashery, S. (2000). Aminoglycosides: Perspectives on mechanisms of action and resistance and strategies to counter resistance. *Antimicrobial Agents and Chemotherapy*, 44(12), 3249–3256. <https://doi.org/10.1128/aac.44.12.3249-3256.2000>
- Krause, K. M., Serio, A. W., Kane, T. R., & Connolly, L. E. (2016). Aminoglycosides: An overview. *Cold Spring Harbor Perspectives in Medicine*, 6(6).  
<https://doi.org/10.1101/cshperspect.a027029>
- Lenhard, J. R., Nation, R. L., & Tsuji, B. T. (2016). Synergistic combinations of polymyxins. *International Journal of Antimicrobial Agents*, 48(6), 607–613.  
<https://doi.org/10.1016/j.ijantimicag.2016.09.014>
- Levison, M. E., & Levison, J. H. (2009). Pharmacokinetics and pharmacodynamics of antibacterial agents. *Infectious Disease Clinics of North America*, 23(4), 791–vii.  
<https://doi.org/10.1016/j.idc.2009.06.008>
- Lund Research Ltd. (2018). *Mann-Whitney U test using SPSS Statistics*. Laerd Statistics.  
<https://statistics.laerd.com/spss-tutorials/mann-whitney-u-test-using-spss-statistics.php>
- Mui, E. (2012, May). *Stanford Health Care aminoglycoside dosing guideline*. Stanford Antimicrobial Safety and Sustainability Program | Antimicrobial Stewardship Resources.  
[http://med.stanford.edu/bugsanddrugs/guidebook/\\_jcr\\_content/main/panel\\_builder\\_584648957/panel\\_0/download\\_1194988017/file.res/Aminoglycoside%20Dosing%20Guide%202019-05-20.pdf](http://med.stanford.edu/bugsanddrugs/guidebook/_jcr_content/main/panel_builder_584648957/panel_0/download_1194988017/file.res/Aminoglycoside%20Dosing%20Guide%202019-05-20.pdf)

Nikaido, H. (2003). Molecular basis of bacterial outer membrane permeability revisited.

*Microbiology and Molecular Biology Reviews : MMBR*, 67(4), 593–656.

<https://doi.org/10.1128/membr.67.4.593-656.2003>

Quintiliani, R. (n.d.). *Pharmacodynamics of antimicrobial agents: Time-dependent vs.*

*concentration-dependent killing*. Antimicrobe.org.

<http://www.antimicrobe.org/h04c.files/history/PK-PD%20Quint.asp>

Sandoval, R., Leiser, J., & Molitoris, B. A. (1998). Aminoglycoside antibiotics traffic to the

Golgi complex in LLC-PK1 cells. *Journal of the American Society of Nephrology :*

*JASN*, 9(2), 167–174. <https://jasn.asnjournals.org/content/9/2/167.long>

Schatz, A., Bugle, E., & Waksman, S. A. (1944). Streptomycin, a substance exhibiting antibiotic

activity against Gram-positive and Gram-negative bacteria. *Proceedings of the Society*

*for Experimental Biology and Medicine*, 55(1), 66–69. [https://doi.org/10.3181/00379727-](https://doi.org/10.3181/00379727-55-14461)

[55-14461](https://doi.org/10.3181/00379727-55-14461)

Schindelin, J., Arganda-Carreras, I., Frise, E., Kaynig, V., Longair, M., Pietzsch, T., Preibisch,

S., Rueden, C., Saalfeld, S., Schmid, B., Tinevez, J. Y., White, D. J., Hartenstein, V.,

Eliceiri, K., Tomancak, P., & Cardona, A. (2012). Fiji: An open-source platform for

biological-image analysis. *Nature Methods*, 9(7), 676–682.

<https://doi.org/10.1038/nmeth.2019>

- Seidl, G., & Nerad, H. P. (1988). Gentamicin C: Separation of C1, C1a, C2, C2a and C2b components by HPLC using isocratic ion-exchange chromatography and post-column derivatisation. *Chromatographia*, 25, 169–171. <https://doi-org.proxy.library.emory.edu/10.1007/BF02316439>
- Serio, A. W., Keepers, T., Andrews, L., & Krause, K. M. (2018). Aminoglycoside revival: Review of a historically important class of antimicrobials undergoing rejuvenation. *EcoSal Plus*, 8(1). <https://doi.org/10.1128/ecosalplus.ESP-0002-2018>
- Smart, M., Rajagopal, A., Liu, W. K., & Ha, B. Y. (2017). Opposing effects of cationic antimicrobial peptides and divalent cations on bacterial lipopolysaccharides. *Physical Review E*, 96(4). <https://doi.org/10.1103/PhysRevE.96.042405>
- Soriano, F., & Greenwood, D. (1979). Action and interaction of penicillin and gentamicin on enterococci. *Journal of Clinical Pathology*, 32(11), 1174–1179. <https://doi.org/10.1136/jcp.32.11.1174>
- Stangroom, J. (2020). *Mann-Whitney U test calculator*. Social Science Statistics. <https://www.socscistatistics.com/tests/mannwhitney/default2.aspx>
- Taber, H. W., Mueller, J. P., Miller, P. F., & Arrow, A. S. (1987). Bacterial uptake of aminoglycoside antibiotics. *Microbiological Reviews*, 51(4), 439–457. <https://www.ncbi.nlm.nih.gov/pmc/articles/PMC373126/>

- Thakur, S., Cattoni, D. I., & Nöllmann, M. (2015). The fluorescence properties and binding mechanism of SYTOX green, a bright, low photo-damage DNA intercalating agent. *European Biophysics Journal : EBJ*, 44(5), 337–348. <https://doi.org/10.1007/s00249-015-1027-8>
- Thermo Scientific. (n.d.). *Hoechst 33342 solution (20 mM)*. ThermoFisher Scientific. <https://www.thermofisher.com/order/catalog/product/62249?us&en#/62249?us&en>
- Todar, K. (2020). *The growth of bacterial populations (page 3)*. Todar's Online Textbook of Bacteriology. [http://textbookofbacteriology.net/growth\\_3.html#:~:text=The%20rate%20of%20exponential%20growth,3](http://textbookofbacteriology.net/growth_3.html#:~:text=The%20rate%20of%20exponential%20growth,3)
- Turnidge, J. (2003). Pharmacodynamics and dosing of aminoglycosides. *Infectious Disease Clinics of North America*, 17(3), 503–v. [https://doi.org/10.1016/s0891-5520\(03\)00057-6](https://doi.org/10.1016/s0891-5520(03)00057-6)
- Vakulenko, S. B., & Mobashery, S. (2003). Versatility of aminoglycosides and prospects for their future. *Clinical Microbiology Reviews*, 16(3), 430–450. <https://doi.org/10.1128/cmr.16.3.430-450.2003>
- Watanakunakorn, C., & Bakie, C. (1973). Synergism of vancomycin-gentamicin and vancomycin-streptomycin against enterococci. *Antimicrobial Agents and Chemotherapy*, 4(2), 120–124. <https://doi.org/10.1128/aac.4.2.120>
- Wei, Z., Shi, X., Lian, R., Wang, W., Hong, W., & Guo, S. (2019). Exclusive production of gentamicin C1a from *Micromonospora purpurea* by metabolic engineering. *Antibiotics (Basel, Switzerland)*, 8(4), 267. <https://doi.org/10.3390/antibiotics8040267>

- Weinstein, M. J., Luedemann, G. M., Oden, E. M., Wagman, G. H., Rosselet, J. P., Marquez, J. A., Coniglio, C. T., Charney, W., Herzog, H. L., & Black, J. (1963). Gentamicin, a new antibiotic complex from *Micromonospora*. *Journal of medicinal chemistry*, 6, 463–464. <https://doi.org/10.1021/jm00340a034>
- Weinstein, M. J., Wagman, G. H., Oden, E. M., & Marquez, J. A. (1967). Biological activity of the antibiotic components of the gentamicin complex. *Journal of Bacteriology*, 94(3), 789–790. <https://doi.org/10.1128/JB.94.3.789-790.1967>
- Wersäll, J., Lundquist, P. G., & Björkroth, B. (1969). Ototoxicity of gentamicin. *The Journal of Infectious Diseases*, 119(4), 410–416. <https://doi.org/10.1093/infdis/119.4-5.410>
- Wilkinson, S. G. (1996). Bacterial lipopolysaccharides - Themes and variations. *Progress in Lipid Research*, 35(3), 283–343. [https://doi.org/10.1016/S0163-7827\(96\)00004-5](https://doi.org/10.1016/S0163-7827(96)00004-5)
- Zhou, Y. F., Tao, M. T., Feng, Y., Yang, R. S., Liao, X. P., Liu, Y. H., & Sun, J. (2017). Increased activity of colistin in combination with amikacin against *Escherichia coli* co-producing NDM-5 and MCR-1. *The Journal of Antimicrobial Chemotherapy*, 72(6), 1723–1730. <https://doi.org/10.1093/jac/dkx038>